TISSUE ENGINEERING: Part A Volume 29, Numbers 7 and 8, 2023 © Mary Ann Liebert, Inc. DOI: 10.1089/ten.tea.2022.0169



Open camera or QR reader and scan code to access this article and other resources online.



ORIGINAL ARTICLE

Sodium Nitroprusside Stimulation of Elastic Matrix Regeneration by Aneurysmal Smooth Muscle Cells

Suraj Bastola, BE,1 Chandrasekhar Kothapalli, PhD,2 and Anand Ramamurthi, PhD, FAHA1

The chronic overexpression of matrix metalloproteases leading to consequent degradation and loss of the elastic matrix with the reduction in tissue elasticity is central to the pathophysiology of proteolytic disorders, such as abdominal aortic aneurysms (AAAs), which are localized rupture-prone aortic expansions. Effecting tissue repair to alleviate this condition is contingent on restoring elastic matrix homeostasis in the aortic wall. This is naturally irreversible due to the poor elastogenicity of adult and diseased vascular cells, and the impaired ability to assemble mature elastic fibers, more so in the context of phenotypic changes to medial smooth muscle cells (SMCs) owing to the loss of nitric oxide (NO) signaling in the AAA wall tissue. In this study, we report the benefits of the exposure of primary human aneurysmal SMCs (aHASMCs) to NO donor drug, sodium nitroprusside (SNP), in improving extracellular matrix homeostasis, particularly aspects of elastic fiber assembly, and inhibition of proteolytic degradation. SNP treatment (100 nM) upregulated elastic matrix regeneration at both gene (p < 0.05) and protein levels (p < 0.01) without affecting cell proliferation, improved gene, and protein expression of crosslinking enzyme, lysyl oxidase (p < 0.05), inhibited the expression of MMP2 (matrix metalloprotease 2) significantly (p < 0.05) and promoted contractile SMC phenotypes in aHASMC culture. In addition, SNP also attenuated the expression of mitogen-activated protein kinases, a significant player in AAA formation and progression. Our results indicate the promise of SNP for therapeutic augmentation of elastic matrix regeneration, with prospects for wall repair in AAAs.

Keywords: abdominal aortic aneurysm, smooth muscle cells, matrix metalloproteases, elastic fibers, nitric oxide, elastin

Impact Statement

Chronic and naturally irreversible enzymatic degradation and loss of elastic fibers are centric to proteolytic disorders such as abdominal aortic aneurysms (AAAs). This is linked to poor elastogenicity of adult and diseased vascular cells, compromising their ability to assemble mature elastic fibers. Toward addressing this, we demonstrate the phenotype-modulatory properties of a nitric oxide donor drug, sodium nitroprusside on aneurysmal smooth muscle cells, and its dose-specific proelastogenic and antiproteolytic properties for restoring elastic matrix homeostasis. Combined with the development of vehicles for site-localized, controlled drug delivery, this can potentially lead to a new nonsurgical approach for AAA wall repair in the future.

¹Department of Bioengineering, Lehigh University, Bethlehem, Pennsylvania, USA.

²Department of Chemical and Biomedical Engineering, Cleveland State University, Cleveland, Ohio, USA.

Introduction

A BDOMINAL AORTIC ANEURYSMS (AAAs) are localized, naturally irreversible expansions of the abdominal aortic wall. Broadly, AAAs develop and grow due to the chronic enzymatic breakdown of the structural matrix (collagen and elastic fibers) of the aortic wall by matrix metalloproteases (MMPs), following an initial injury stimulus. However, the condition is highly multifactorial in its etiology, additionally involving the infiltration of leucocytes and production of proinflammatory cytokines, vascular smooth muscle cell (VSMC) apoptosis, loss of nitric oxide (NO) signaling, endothelial dysfunction, and phenotypic modulation of VSMCs between contractile and synthetic phenotypes.^{1,2}

The breakdown of the matured crosslinked elastic matrix, which imparts stretch and recoil properties to the aortic wall, is a critical determinant of abnormal vessel expansions as this naturally irreversible phenomenon leads to loss of aortic wall elasticity, weakening, and ultimately potentially fatal rupture. This is linked to the poor synthesis of the elastin (ELN) precursor—tropoelastin—by the adult and diseased vascular cells, and the inability of these cell types to replicate the biocomplexity of the elastic fiber assembly process that occurs primarily during the postneonatal period. The problem of poor elastic fiber regeneration and repair in the AAA wall is exacerbated by the chronically upregulated production of elastolytic proteases such as MMP2 and MMP9, which further limits the accumulation of new elastic matrix.

In the absence of any proven therapies to reverse AAA pathophysiology and more specifically, restore elastic matrix homeostasis, slowing or arresting the growth of small (<5 cm diameter) AAAs to a large, prerupture stage, mandating risky surgical intervention, is not currently possible. The availability of nonsurgical matrix regenerative therapies would have a significant impact in enabling this.

In the cardiovascular system, NO, a biological regulator molecule, has been shown to act by cyclic guanosine monophosphate (cGMP)-dependent or cGMP-independent pathways to regulate several critical cellular processes.^{4,5} Separately, mitogen-activated protein kinase (MAPK) proteins, such as c-Jun N-terminal kinase (JNK), extracellular signal-regulated kinases (ERKs), and p38, are highly upregulated in AAAs.^{6,7} These MAPK proteins regulate downstream expression of MMPs and proteolytic disruption of the vessel structural extracellular matrix (ECM). We have published that attenuating JNK significantly upregulates elastic fiber neoassembly and reduces MMP activity by aneurysmal SMCs.8 In light of evidence that endogenously generated NO downregulates MMPs and suppresses JNK phosphorylation and activation, in this work, we have sought to investigate if exposure of primary human aneurysmal SMCs (aHASMCs) to a NO donor drug, sodium nitroprusside (SNP), is a useful therapeutic modality to restore ECM homeostasis.

Materials and Methods

aHASMCs isolation and culture from AAA tissue biopsies

AAA tissues were obtained from patients undergoing open surgical repair of an AAA under an IRB protocol approved by the Cleveland Clinic, Ohio. Primary aHASMCs

were isolated and characterized as previously described. 10 First, the intimal layer composed of endothelial cells was scraped off from the AAA tissue, and the medial layer was separated from the underlying adventitial layer and adipose tissue. Then, the sliced tissue was further cut into pieces of roughly 5 mm² and subjected to a two-step enzymatic digestion process in Dulbecco's modified Eagle's medium and Ham's F-12 medium (DMEM/F12; Thermo Fisher Scientific, Waltham, MA), first with 125 U/mg collagenase type I (Worthington Biochemicals, Lakewood, NJ) for 20 min at 37°C, and then with 3 U/mg elastase (Worthington Biochemicals) for 1 h in a temperature-controlled shaker at 37°C. The digestates were then centrifuged (1245 rpm, 10 min) and transferred to a 10-cm² culture dish (six-well plate). The culture surface of each well was scratched with a sterile scalpel blade to create grooves for cell attachment.

Primary aHASMCs, derived by outgrowth of the digestates, were cultured for 14–21 days in DMEM/F12 medium supplemented with 20% v/v fetal bovine serum (FBS; Gibco, Waltham, MA) and 1% v/v penicillin–streptomycin (Pen–Strep; Thermo Fisher Scientific) and then transferred to a T-25 flask for further propagation. The aHASMCs from passages 2 to 6 were used for experiments.

SNP IC₅₀ determination

SNP (Sigma, Burlington, MA) cytotoxicity was determined using a 3-(4,5-dimethylthiazol-2-yl)-2,5-diphenyl tetrazolium bromide (MTT) assay (Abcam, Waltham, MA). Two days postseeding, aHASMC cultures (3×10^4 cells/well, six-well plates, n=3), were treated with SNP (100 pM–10 mM) reconstituted in DMEM/F12 medium containing 1% v/v Pen–Strep and 2% (or 10%) v/v FBS for the 24 h; control cultures received no SNP. MTT reagent (0.5 mg/mL in phosphate-buffered saline [PBS]) was then added to each well and incubated for 3 h to allow the formation of a blue crystalline formazan product. The formazan was solubilized using 300 µL of dimethyl sulfoxide, and 200 µL of each sample was taken in a 96-well plate, and absorbance was measured at a wavelength of 570 nm.

Cytokine injury cell culture model

The aHASMCs were seeded in chamber slides for 48 h and serum starved in DMEM/F12 medium containing 2% v/v FBS for 3 h. Immediately after serum starving, aHASMC cultures were treated with a cocktail of $10\,\text{ng/mL}$ of tumor necrosis factor-alpha (TNF α ; Thermo Fisher Scientific) and $10\,\text{ng/mL}$ of interleukin-1 beta (IL-1 β ; R&D Systems, Minneapolis, MN) for various time points (0 min, 30 min, 1 h, 2 h, 3 h, 24 h) to determine the optimal time for upregulating these proteolytic conditions as a function of MMP2 expression. MMP2 expression in each culture was visualized using immunofluorescence (IF) imaging with an Olympus IX51 fluorescence microscope (Olympus America, Center Valley, PA) as described in our experimental design section below.

Design of cell culture experiments

For cell culture experiments, aHASMCs were seeded at a density of 3×10^4 – 5×10^4 cells/well in a 6-well or 15×10^3 cells/well in 12-well plate/2-well chamber slides and

cultured in DMEM/F12 containing 10% v/v FBS for 7 days. On day 7, the cells were serum starved in DMEM/F12 containing 2% v/v FBS for 3 h, followed by 3 h of cytokine treatment with a cocktail of TNFα (10 ng/mL) and IL-1β (10 ng/mL). This was followed by treating the cells with various doses of SNP (100 nM, 10 nM, 1 nM, and 100 pM) for 7 days for gene and protein studies (or 14 days for elastic matrix quantification). The treatment was done every day by replenishing the DMEM/F12 media with a freshly prepared medium containing SNP in each of the culture wells. Control wells received media change each day without SNP treatment. Gene expression analysis was done using realtime polymerase chain reaction (RT-PCR) and quantitative polymerase chain reaction (qPCR) SMC biology array, whereas protein expression was quantified using western blot (WB), IF, MAPK array, and biochemical assays for elastin, collagen, and DNA quantification. The overall experimental design is shown in Supplementary Figure S1.

Real-time polymerase chain reaction

Relative levels of gene expression between cases were determined by real-time PCR. The total mRNA for this experiment (n=6) was extracted after 2 weeks of culture using the RNeasy Mini Kit (Qiagen, Valencia, CA) as per the manufacturer's instructions. The total mRNA concentration was determined by Nanodrop 2000 spectrophotometer (Thermo Fisher Scientific, Wilmington, DE). MRNA (200 ng) was reverse transcribed to cDNA using the iScript cDNA Synthesis Kit (Bio-Rad, Hercules, CA) in a thermocycler as instructed by the manufacturer. The expression of SMC-specific genes was quantified using SYBR® Green master mix and target-specific primers (RealtimePrimers; Elkins Park, PA) in Quantstudio[®] 3 (Applied Biosystems; Thermo Fisher Scientific). The relative gene expression of each target was determined by using the $\Delta\Delta$ Ct method as explained by Livak and Schmittgen. 11 Data were normalized to the endogenous reference gene (18s). The list of primers and their respective sequences used in this study are shown in the Supplementary Table S1.

WB analysis

The protein expression in each sample was assessed semiquantitatively using WB analysis. aHASMCs were harvested in RIPA buffer (Thermo Fisher Scientific) containing 1% v/v HaltTM protease inhibitor and phosphatase inhibitor (Thermo Fisher Scientific). Total protein expression was

determined using a colorimetric Bicinchoninic Acid (BCA) Assay Kit (Thermo Fisher Scientific). The protein samples (2 μg) mixed with the loading buffer and a reducing agent were loaded in 10% or 4–12% NuPAGE™ Bis-Tris gels. SeeBlue® prestained ladder was used for molecular weight approximation. The gel was then subjected to sodium dodecyl sulfate–polyacrylamide gel electrophoresis (SDS-PAGE; Thermo Fisher Scientific) and transferred to a nitrocellulose membrane using iBlot® Western Blotting System (Invitrogen). The transferred membranes were blocked, and incubated overnight with primary antibodies (Table 1), followed by secondary antibody incubation (with IRDye® 680LT goat-anti-rabbit secondary antibody in (1:15,000 dilutions) and IRDye® 800CW goat anti-mouse secondary antibody (1:20,000 dilution) as published.^{8,12}

Gelatin zymography for MMP2 activity

The enzyme activity of MMP2 was determined by gel zymography. Briefly, $2\,\mu g$ of protein was loaded in each well alongside MMP2 standard. Then the gels were run in an electrophoresis unit at $125\,V$ as discussed in our WB experiments. The gels were then renatured in 2.5% Triton X-100, developed in the $1\times Novex$ development buffer and stained with SimplyBlue SafeStain. The destaining of the gels was done in DI water for $72\,h$. After destaining, MMP2 bands on a dark background was quantified using ImageJ software.

SMC biology PCR array

For SMC biology-focused gene expression analysis of cultured aHASMCs, a Human qPCR Array Kit (ScienceCellTM Research Laboratories, Carlsbad, CA) was used. A limited SNP dosage (0 M, 100 nM) study was performed to compare the gene expression profile of a total of 88 genes (no replicates during analysis) relevant to SMC biological function, contraction, phenotypic switching, and ECM synthesis. The mRNA (35 ng) from our RT-PCR sample was pooled from each sample/per group (n=6) to comprise a final concentration of 210 ng mRNA. The mRNA was then reverse transcribed to cDNA using the iScript cDNA Synthesis Kit. The cDNA amplification was done in Quantstudio 3 using KAPA SYBR fast qPCR master mix $(2 \times)$ ROX low (Roche Sequencing and Life Sciences, Indianapolis, IN). Gene expression was analyzed using the $\Delta\Delta$ Ct method. The data were normalized to the geometric mean of five different housekeeping genes (β-Actin, GAPDH, LDHA, NONO,

TABLE 1. DETAILS OF PRIMARY ANTIBODIES USED IN WESTERN BLOT AND IMMUNOFLUORESCENCE

Protein	WB dilution (v/v)	IF dilution (v/v)	Catalog No.	Source
MMP2	1:1000	1:200	ab92536	Abcam
TIMP1	1:1000	1:200	bs-0415R	Thermo Fisher Scientific
TIMP2	1:1000	1:200	ab180630	Abcam
TIMP4	1:1000	1:200	ab38987	Abcam
LOX	1:1000	1:50	ab31238	Abcam
JNK	1:1000	NA	44-682G	Thermo Fisher Scientific
ERK	1:1000	NA	9102S	Cell Signaling Technology
FBN	1:1000	1:100	PA5-99225	Thermo Fisher Scientific
ELN	1:1000	1:100	ab217356	Abcam
β-Actin	1:2000	NA	MAB8929	Thermo Fisher Scientific

IF, immunofluorescence; WB, western blot.

PPIH) and presented as log₂-fold change to determine the multiplicative factor of upregulation or downregulation of the target gene versus control.

LIVE/DEAD assay for cell viability

To assess the effect of SNP dose on aHASMC viability, a LIVE/DEADTM Viability/Cytotoxicity Kit (Thermo Fisher Scientific) was used. The SNP doses were 500 nM, 100 nM, and 1 μ M. For this experiment, 15×10^3 cells/well were seeded in a 12-well plate and cultured for 7 days. Cells were then serum starved, and cytokine treated as explained in our experimental design section. Following the cytokine treatment, cells were then treated with SNP for 24 h. Subsequently, the cells were stained with calcein-AM and ethidium homodimer-1, as per the manufacturer's instructions, to determine the percentage of viable and dead cells.

DNA assay for cell proliferation

The effect of different SNP doses on aHASMC proliferation over 21 days of culture was determined using a Hoechst-33248 dye-based fluorometric DNA assay as described earlier. Briefly, in this dose escalation study, aHASMCs were seeded in six-well plates $(5\times10^4~\text{cells/well})$ and treated with SNP at doses of 100, 250, and 500 nM. The cells were cultured for 21 days, harvested using Pi Buffer (50 mM Na₂HPO₄, 2 mM EDTA, 0.3 mM NaN₃), and sonicated to lyse the cells. Cell counts in each sample were calculated based on the assumption that each cell contains 6 pg of DNA. 14

Fastin assay for elastic matrix quantification

A FASTIN assay (Accurate Chemical and Scientific Corp. Westbury, NY) was used to quantify the total elastin deposited by cells as per the manufacturer's protocol. Briefly, 500 µL of the cell lysates harvested in Pi buffer (as discussed in the DNA assay for cell proliferation section) were digested in 1.5 M oxalic acid for 1.5 h at 95°C to extract soluble alpha-elastin. The digested samples were centrifuged at 14,000 g, and the supernatant was transferred to a new 1.5-mL centrifuge tube. The pellet containing insoluble elastin was further digested in 0.25 M oxalic acid (1 h, 100°C) and centrifuged at 14,000 g to convert it into a soluble form. The sample from the second digestion was pooled with the supernatant from the first digestion. Following the manufacturer's protocol, elastin content was calculated using colorimetric absorbance reading at 513 nm. Data were presented by normalizing them with their corresponding DNA contents.

Hydroxyproline assay for collagen quantification

Collagen matrix content was estimated by quantifying total hydroxyproline (OH-Proline) content in the cell culture samples. 15,16 Briefly, for this experiment, 500 μL of the cell lysates harvested in Pi buffer (as discussed in the DNA assay for cell proliferation section) were hydrolyzed in 12 M HCl at 95°C for 24 h. Cells were then vortexed for 3 min. Colorimetric analysis of OH-proline was done by taking 25 μL of the hydrolyzed sample in a 96-well plate and incubating them with $100\,\mu L$ of oxidizer solution (mixture of Chloramine T, 1-propanol, citrate buffer) for

30 min in room temperature and then with Erlich's solution (DMAB, 1-propanol, and 70% perchloric acid) for 45 min at 65°C. All reagents were obtained from Sigma (St. Louis, MO) Absorbance was measured at 550 nm. Collagen amounts were calculated based on the assumption that each fibrillar collagen contains $\sim 13.5\%$ w/w of OH-proline.

Human desmosine enzyme-linked immunosorbent assay

Desmosine in the aHASMC cultures was quantified using a Human Desmosine Enzyme-Linked Immunosorbent Assay (ELISA) Kit (MyBioSource, San Diego, CA). aHASMCs were harvested in PBS on day 21 and centrifuged at 1000 g for 15 min and the supernatant was transferred to a new microcentrifuge tube. The cell pellets were subjected to three freeze/thaw cycles and then resuspended in PBS. The resuspended cell pellets were ultrasonicated (20 kHz, 20% amplification, 30 s on, 10 s off) and repelleted by centrifuging (1000 g, 15 min, 2–8°C). A BCA assay was used to quantify the total protein. The samples were then immediately subjected to ELISA assay following the manufacturer's protocol.

MAPK phosphorylation antibody array

To determine the effect of limited SNP dose (100 nM vs. control) on the expression of phosphorylated (activated) MAPKs, a human MAPK phosphorylation antibody array (ab211061; Abcam) was used. For the experiment, 5× 10⁴ cells/well were seeded in a six-well plate and cultured for 14 days. At that time, the cells were serum-starved for 3h, then treated with a cocktail containing 10 ng/mL of TNFα and 10 ng/mL of IL-1β, with or without SNP (100 nM) for 10, 15, and 30 min. Cells that were neither treated with SNP nor with the cytokines served as controls. Cell lysates were harvested in a lysis buffer as provided and recommended by the manufacturer. BCA assay was done to quantify the total protein concentration in each sample. For the MAPK array experiment, briefly, the antibody array membranes were blocked in a blocking buffer (2 mL) for 30 min at 25°C before incubating them overnight at 4°C with 150 μg of protein samples.

The membranes were washed using the wash buffers and were then sequentially incubated with a detection antibody cocktail and 1×horseradish peroxidase anti-rabbit IgG overnight at 4°C. Finally, a cocktail of detection antibodies was added to the membrane and the membrane was imaged in ChemiDoc MP (Bio-Rad).

Atomic force microscopy analysis

The aHASMCs (10⁴ cells/well) were cultured on 2D collagen-coated substrates for up to 48 h in DMEM/F12, containing 0 (Control), 1, 10, or 100 nM SNP. Medium was changed once every 24 h with fresh SNP addition. Cells were maintained at 37°C throughout the live cell nanoindentation assay. An MFP-3D-Bio atomic force microscopy (AFM; Asylum Research, Oxford Instruments, Santa Barbara, CA) mounted on an inverted fluorescence microscope (Nikon Eclipse Ti), and tipless AFM cantilevers modified by gluing a 5-µm polystyrene bead, were used for the measurements. The spring constant was determined

from the force/distance curves using the thermal calibration method in a clean culture dish containing warm media. For each condition, cells were indented between the nuclei and edges, and force curves were obtained at random locations on each cell in force-volume mode at an approach/retraction velocity of $5 \, \mu \text{m/s}$.

A Hertz's contact model for spherical indenters, given by $F = 4E_Y \sqrt{R\delta^3/3(1-\mu^2)}$, was used to determine Young's modulus from these force curves, where F is the indentation force, E_Y is Young's modulus, μ is Poisson's ratio (~ 0.5 for cells), R is the tip radius (2.5 µm), and δ is the indentation depth ($\sim 500 \, \mathrm{nm}$). The force of adhesion $(F_{\rm ad})$ —the force required to separate the AFM tip and cell surface—was obtained directly from the force/deflection curve during the retraction mode. The tether forces (F_T) were obtained from the force steps displayed in the retraction curves. The apparent membrane tension (T_M) , the force needed to deform a membrane, was calculated from such tether forces using $T_M = F_T^2/8\pi^2 k_B$, where k_B is the bending stiffness of membranes (assumed to be $\sim 0.1 \text{ pN/}\mu\text{m}^{17}$). Similarly, the tether radius (R_T) that describes the plasma membrane to cytoskeleton connection was calculated as $R_T = 2\pi k_B/F_T$. Finally, the mean surface roughness (R_a) of each cell, characterized as the arithmetic mean of the deviations in height from the line mean value, was obtained from randomly selected areas on the cell membrane.

IF-based detection of ECM homeostasis proteins

For IF labeling, 15×10^3 cells/well were cultured in a twowell Permanox chamber slide (Nalge Nunc International, Rochester, NY) as previously published. 18 Briefly, 7 days postseeding, cells were serum starved and cytokine treated, as specified in the experimental plan. The cells were then subjected to SNP treatment for 7 days for signaling MAPK proteins (JNK, p-JNK, ERK, p-ERK) with and without 2-phenyl-4,4,5,5-tetramethylimidazoline-1-oxyl 3-oxide (PTIO;Sigma), which is an NO scavenger; transmembrane proteins (including MMP2, MMP9; TIMP1, TIMP2, TIMP4); and 14 days for ECM proteins (ELN, lysyl oxidase [LOX], fibrillin1 [FBN1]), for total culture times of 14 or 21 days, respectively. At the end of treatment, cells were washed twice with PBS and fixed in 4% w/v paraformaldehyde containing 0.1% v/v Triton X-100 (VWR Scientific, West Chester, PA) for 30 min at room temperature for transmembrane proteins, and with ice-cold methanol for 20 min at 4°C for ECM proteins.

Next, the fixed cells were blocked in 5% v/v goat serum (Gibco) for 30 min. The cells were then incubated overnight with primary antibodies against MMP2, MMP9, TIMP1, TIMP2, TIMP4, ELN, LOX, FBN, JNK, p-JNK, ERK, and p-ERK (Table 1). The expression of these proteins was visualized using either goat anti-rabbit or goat anti-mouse IgG (Alexa Fluor[®] 594 or Alexa Fluor[®] 633; Thermo Fisher Scientific). The nucleus was stained using 4′,6-diamidino-2-phenylindole (Vector Laboratories, Burlingame, CA).

Transmission electron microscopy

Transmission electron microscopy (TEM) was used to quantitively assess the newly deposited elastic matrix by aHASMCs and compare them with the untreated controls. The aHASMCs were cultured in two-well Permamox® chamber slides (Sigma) for 21 days. On day 7 of culture, cells were serum starved and cytokine injured followed by SNP treatment for 14 days (as described in the experimental plan). On day 21, cells were washed three times with PBS and fixed in a buffer containing 4% w/v paraformaldehyde, 2.5% w/v glutaraldehyde, and 0.1 M sodium cacodylate buffer for 1 h at room temperature, followed by overnight incubation at 4°C. The samples were then postfixed with 1% w/v osmium tetroxide for 1 h, dehydrated in 50–100% ethanol series, and embedded in the Epon 812 resin before sectioning it and placing them on the copper grids. After that, samples were stained with uranyl acetate and lead citrate before imaging them at multiple magnifications as described in our previously published work.⁸

Statistical analyses

Statistical data analyses were performed using GraphPad Prism[®]. The statistical comparison between the groups was done using one-way ANOVA or Student's *t*-test as required. Comparison of different treatment groups with the control was tested with Dunnett's *post hoc* analysis and multiple comparisons between the groups were tested with the Tukey–Kramer test. Data are presented as mean±standard deviation unless specified, with a *p*-value <0.05 deemed for statistically significant difference.

Results

Cell viability and IC50 of SNP

At SNP doses of 10 mM, 100 μ M, 1 μ M, 10 nM, and 100 pM under low serum conditions (DMEM/F12 with 2% v/v FBS), aHASMC viabilities were 3.2% \pm 0.5%, 90.8% \pm 5.6%, 84.1% \pm 8.7%, 83.1% \pm 17.4%, and 90.8% \pm 5.8%, respectively. Under higher serum conditions (DMEM/F12 with 10% v/v FBS), cell viabilities at the same SNP doses were 0%, 41.5% \pm 6.4%, 55.08% \pm 6.4%, 87.3% \pm 12.8%, and 96.6% \pm 6.7%, respectively (Supplementary Fig. S2). The IC₅₀ values of SNP were calculated to be 0.3 mM and 5.4 μ M in low-serum and high-serum conditions, respectively. Based on this experiment, the acceptable (noncytotoxic) dose range for *in vitro* SNP treatment was determined to be between 100 nM and 100 pM, as prepared in DMEM/F12 medium containing 10% v/v FBS.

Cytokine activation of aHASMCs

MMP2 expression increased significantly at 2, 3, and 24 h of cytokine treatment versus control or those treated with cytokines for only 30 min (p<0.0001) in aHASMC cultures. In addition, MMP2 expression was significantly upregulated in cultures subjected to 2, 3, and 24 h of cytokine exposure (longer exposure) versus 1 h of cytokine exposure (p=0.03). MMP2 expression peaked at 3 h of cytokine exposure and remained unchanged between cultures with longer cytokine exposure times (Fig. 1).

Effect of SNP on ECM homeostasis and aHASMC markers

Figure 2 shows the gene expression in cytokine-injured aHASMC cultures following treatment with a range of SNP

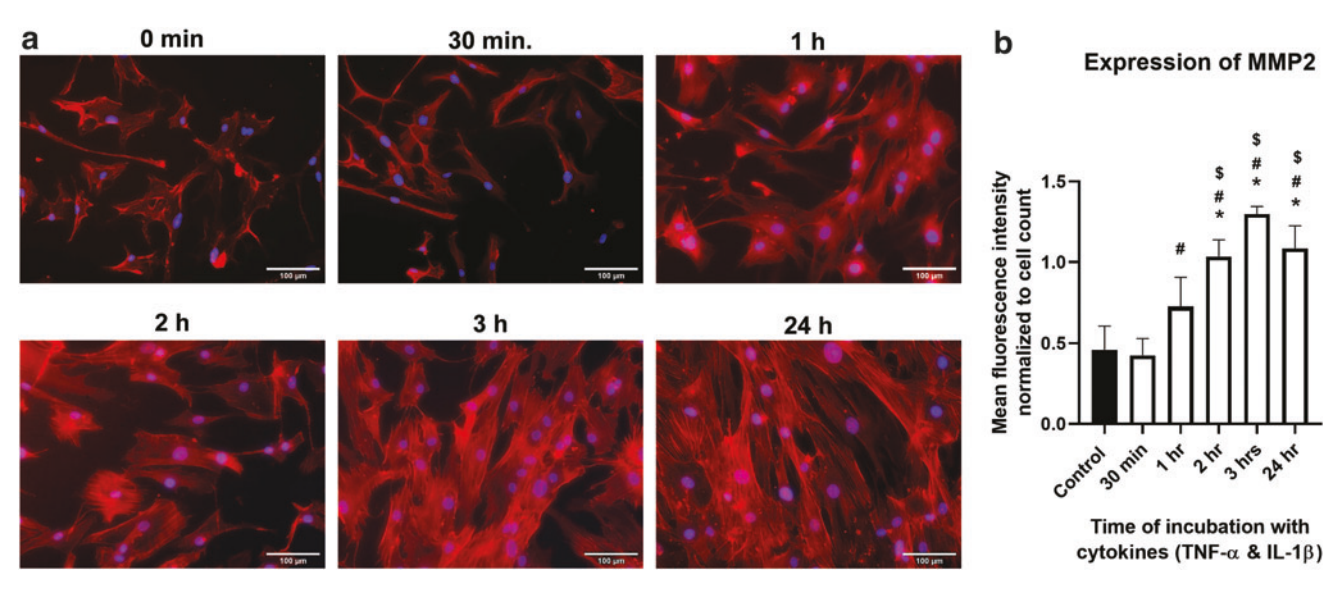


FIG. 1. Effect of cytokine exposure duration on the activated phenotype of aHASMCs. (a) IF detection of MMP2 expression (red) in response to cytokine injury on aHASMCs; DAPI-labeled nuclei appear *blue*. Scale bar = $100 \,\mu\text{m}$. (b) The fluorescence intensity of MMP2 expression from the IF images was quantified, normalized to the respective nuclei count, and represented as mean \pm SD. *, # And \$ denote p = 0.05 compared with controls, 30 min of cytokine treatment, and 24 h of cytokine treatment, respectively (n = 4 cultures/case). aHASMCs, adult human aneurysmal smooth muscle cell; DAPI, 4',6-diamidino-2-phenylindole; IF, immunofluorescence; MMP, matrix metalloprotease; SD, standard deviation. Color images are available online.

doses. Figure 2a shows the expression of SMC marker genes. Smooth muscle alpha-actin (ACTA) and desmin (DES) expression by aHASMCs was downregulated at all SNP doses ($p\!=\!0.001$ and 0.02 vs. control, respectively), and myosin heavy chain (MYH11) expression was reduced at all SNP doses, except 100 pM ($p\!=\!0.05$ vs. control). The gene expressions of end-stage contractile SMC phenotypic markers, smoothelin (SMTH), and calponin (CNN) remained unaffected by SNP.

Furthermore, MMP2 gene expression was significantly decreased upon SNP treatment versus controls (p < 0.05vs. control: Fig. 2b). Among TIMPs (Fig. 2b), TIMP1 gene expressions remained unchanged at all dosages, while TIMP2 was significantly upregulated only at 100 nM (p=0.006) and TIMP4 was downregulated at 100 pM (p=0.03 vs. control), but remained unchanged at higher doses. ELN gene expression was significantly higher at the 100 nM SNP (p=0.05 vs. control), and LOX gene expression was upregulated at 100 pM and 100 nM (p = 0.03vs. control) (Fig. 2b). In addition, the gene expression ratio of TIMP1 to MMP2 was upregulated at 10 nM (p=0.01) and $100 \,\mathrm{nM}$ (p=0.001) by $\sim 1.8 \pm 0.4$ and $\sim 2.03 \pm 0.2$ -fold, respectively, and the gene expression ratio of TIMP2 to MMP2 was upregulated at 100 nM (p = 0.0001) by $\sim 5 \pm 0.8$ -fold. However, there was no significant change in TIMP4 to MMP2 gene expression ratios with SNP treatment.

On the other hand, the gene expression ratio of *ELN* to collagen type III alpha 1 (*COL3A1*) was significantly upregulated at $100 \, \text{nM}$ by $\sim 5 \pm 0.5$ -fold (p = 0.03), whereas, gene expression of *ELN* to collagen type I alpha 1 (*COL1A1*) did not change significantly (Fig. 2d). In addition, relative gene expression of *FBN1* was downregulated at $100 \, \text{pM}$ and $1 \, \text{nM}$ of SNP (p = 0.006 vs. control) but

remained unchanged at higher doses, and COL1A1 genes were unaffected by SNP treatment (Fig. 2c). In contrast, COL3A1 was significantly downregulated at all SNP doses ($p\!=\!0.03$ vs. control), except at 100 pM SNP (Fig. 2c). Among various MAPKs (Fig. 2c), gene expression of ERK1 was downregulated at all SNP doses ($p\!=\!0.01$ vs. control), except at 10 nM. ERK2 gene expression was downregulated at 100 pM and 100 nM ($p\!=\!0.02$ vs. control), whereas JNK1 and JNK2 gene expression remained unchanged at all SNP doses.

Effect of SNP on ECM homeostasis protein expression

The dose-dependent effects of exogenous SNP on the synthesis of key ECM homeostasis proteins (MMPs, TIMPs), cell signaling MAPK proteins (JNK, ERK), and ECM proteins (LOX, FBN1) (Fig. 3) were semiquantitatively assessed using WB analysis. At all tested doses, SNP suppressed MMP2 levels ($p\!=\!0.001$ vs. control) (Fig. 3a). Although TIMP1 (28 kDa) and TIMP2 (24 kDa) remained undetected in WBs, TIMP4 was detected in two distinct bands—26 and 62 kDa (Fig. 3b). The expression of TIMP4 (both isoforms) appeared higher in SNP-treated cultures, but this increase was not statistically higher than in control cultures.

At the analysis time points, the expression of MAPK proteins, including JNK (Fig. 3c), ERK1 (44 kDa), and ERK2 (42 kDa) (Fig. 3d) was not significantly altered by SNP treatment. Similarly, FBN1 (312 kDa) was not significantly different (Fig. 3e); however, LOX (47 kDa) was upregulated at 100 pM SNP dose (p=0.006), 1 nM dose (p=0.04), and 100 nM dose (p=0.004) (Fig. 3f). Additionally, gelatin zymography of MMP2 showed significant downregulation of enzyme activity at SNP doses of 1, 10, and 100 nM (p=0.04) (Fig. 3g).

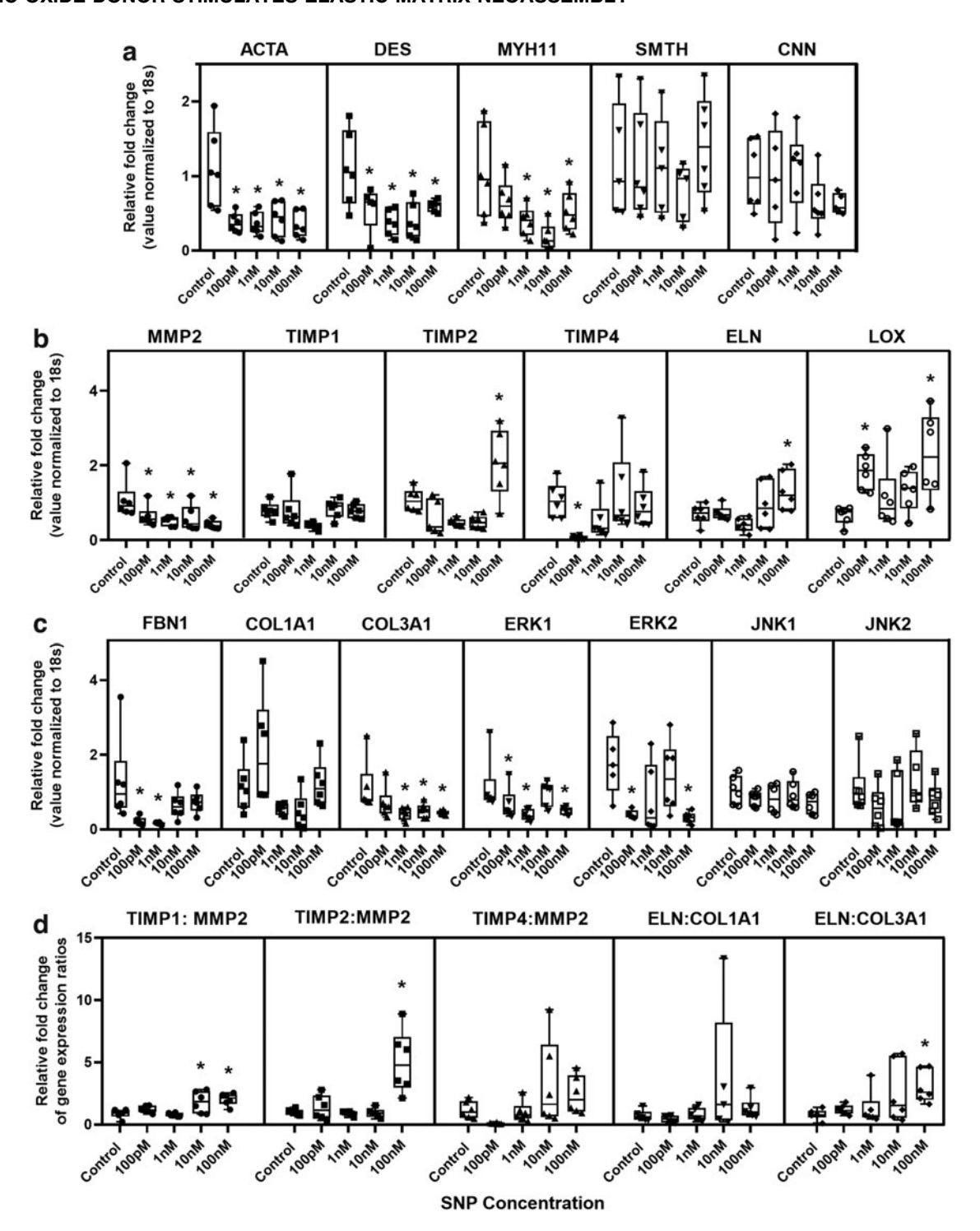


FIG. 2. (a–c) SNP effects on gene expressions of various phenotypic markers, ECM homeostasis proteins, and MAPK proteins in aHASMC cultures. (d) Shows the gene expression ratio of TIMP1 to MMP2, TIMP2 to MMP2, TIMP4 to MMP2, TIMP4 to T

Effect of SNP on aHASMC gene expression profile at proregenerative/antiproteolytic dose

RT-PCR and WB results indicated significant matrix regenerative and antiproteolytic benefits of SNP in aHASMC cultures at the 100 nM dose. A human qPCR gene analysis array was performed at this singular dose to assess SNP

effects more broadly on expression profiles of different functionally grouped genes. Among the analyzed genes, the contractile SMC markers, *ACTA* and caldesmon 1 (*CAD1*), were downregulated upon SNP treatment (Fig. 4a). SNP also downregulated genes known to induce synthetic-like SMC phenotype and regulate the growth, proliferation, and migration of SMCs, such as myocardin (*MYOD*), GATA-binding

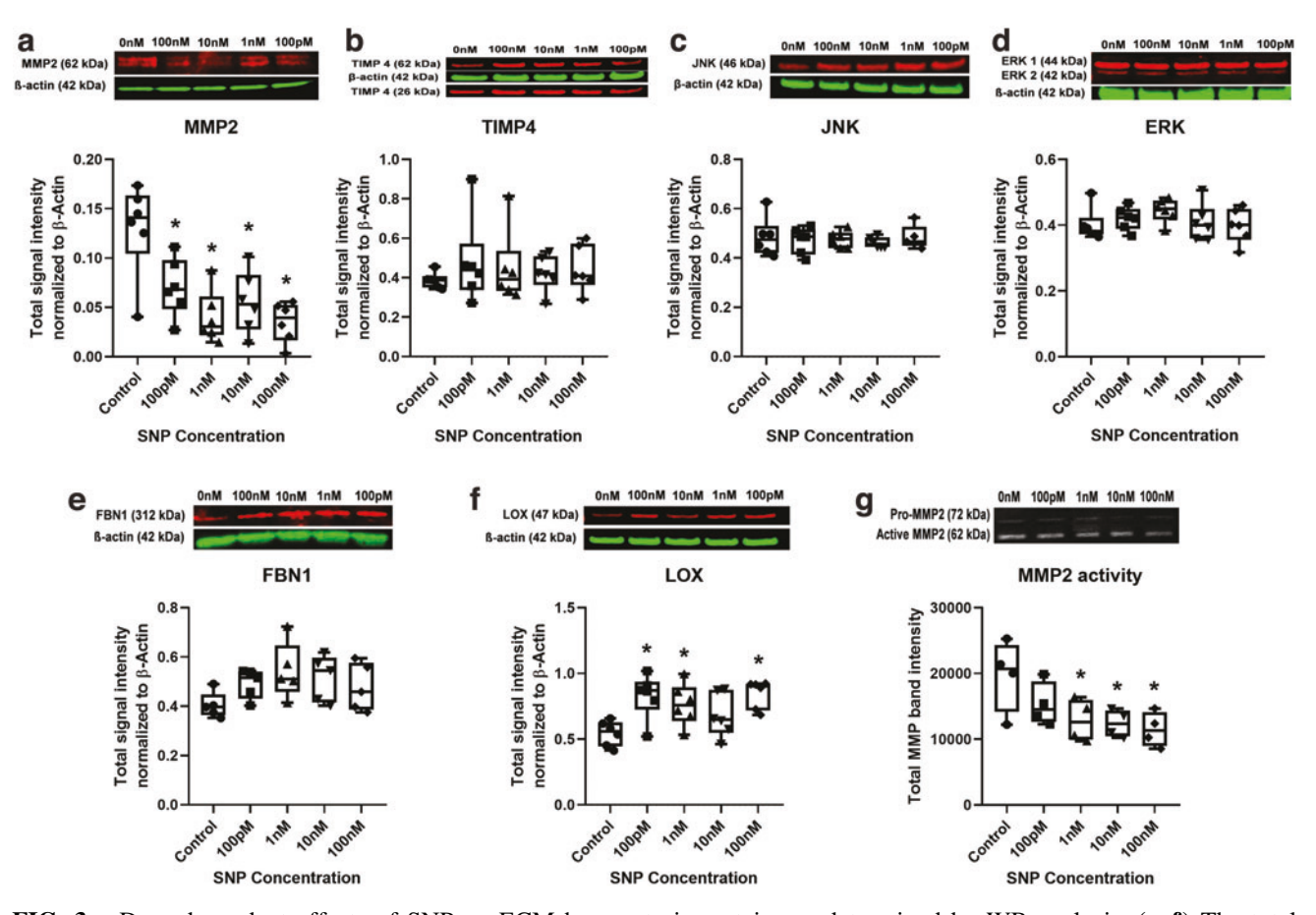


FIG. 3. Dose-dependent effects of SNP on ECM homeostasis proteins as determined by WB analysis. (a–f) The total signal intensity of each analyzed protein was further normalized to β -actin expression and shown, along with representative WB gel blots. (g) Representative gelatin zymography showing total MMP2 activity. y-Axis represents total MMP2 band intensity obtained from the gels (n=4). Data are presented as mean ± SD of results obtained for n=6 cultures/condition with statistical differences (p<0.05) versus untreated controls indicated by *. WB, western blot. Color images are available online.

protein 6 (*GATA6*), Hairy/enhancer-of-split related with YRPW motif protein 2 (*HEY2*), monocyte enhancer-binding factor 2B (*MEF2B*), Notch receptor 1 (*NOTCH1*), and Notch receptor 3 (*NOTCH3*) (Fig. 4b). Furthermore, there was an increase in *ELN* expression and comparatively lower expression of collagen type I (*COL1A1* and *COL1A2*) and collagen type III (*COL3A1*) genes (Fig. 4c). Collagen type IV gene (*COL4A1*) expression was highly reduced.

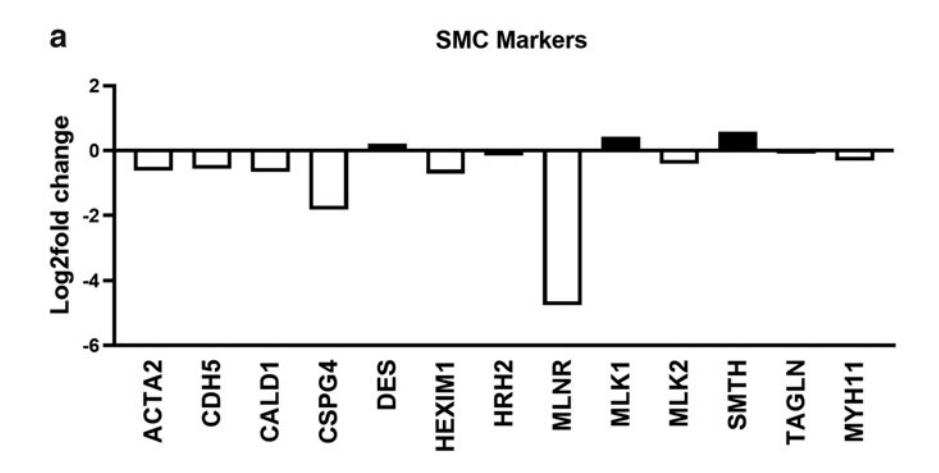
Effect of SNP on cell viability

We determined the cytotoxicity of SNP doses in a range of 100 nM to 1 μM to select a safe dose range for our dose escalation study done to determine the effects of SNP on cell proliferation and elastic matrix synthesis. Results from the LIVE/DEAD assay showed a significant reduction in cell viability at 1 μM dose of SNP ($p\!=\!0.0001$). Cell viability was not adversely impacted at 500 and 100 nM of SNP relative to controls but was significantly higher than in the cultures treated with 1 μM of SNP ($p\!=\!0.0001$ vs. 1 μM) (Supplementary Fig. S3). The percentage of live cells in cultures treated with 1 μM , 500 nM, and 100 nM of SNP was 50.1% $\pm\,20.6\%$, 90.3% $\pm\,3.2\%$, and 98.1% $\pm\,4.6\%$, respectively.

Effect of SNP on cell proliferation and ECM synthesis

Based on the initial findings of LIVE/DEAD assay and the proregenerative and antiproteolytic effects of SNP at the 100 nM dose, SNP effects on matrix synthesis were evaluated at this and higher doses (250, 500 nM). No significant difference was seen in cell proliferation between control and 100 nM SNP-treated cultures although higher SNP doses induced significantly robust proliferation of aHASMCs versus controls (p = 0.002 and 0.005 for 250 and 500 nM, respectively) and 100 nM SNP dose (p = 0.01 and 0.02 for 250 and 500 nM, respectively) (Fig. 5a). The total elastic matrix content in the SNP-treated cultures were all significantly higher than in the controls (p=0.0004, 0.0001, 0.0001 vs. controls for 100, 250, and 500 nM of SNP, respectively; Fig. 5b). There were no significant SNP dosedependent differences in total elastin amounts within the groups. On a cell count-normalized basis, elastic matrix amounts were deemed significantly higher than controls only in cultures treated with 100 nM of SNP (p=0.01 vs. control) (Fig. 5c).

On the other hand, the hydroxyproline assay did not detect any collagen in the samples. In addition, the total desmosine (normalized to total protein concentration)



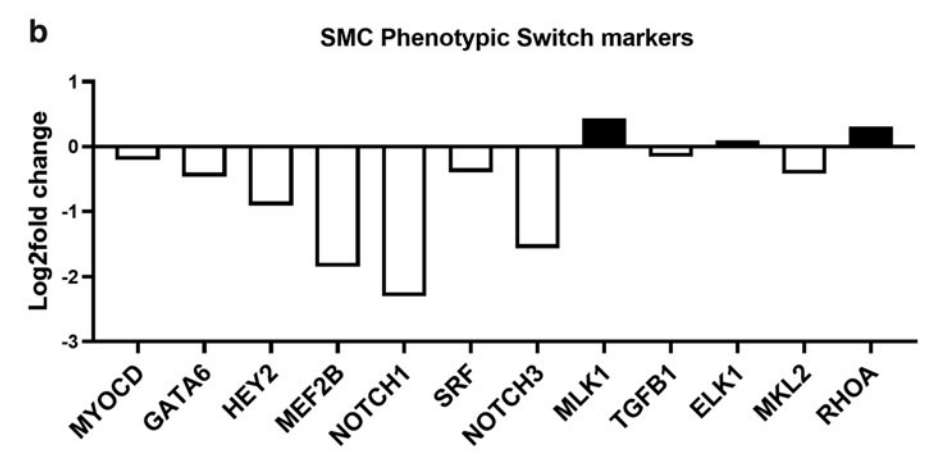
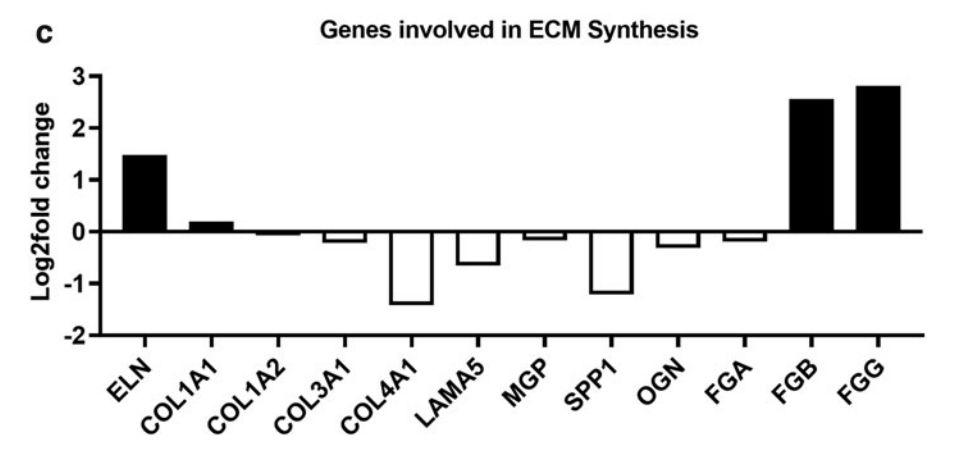


FIG. 4. A human SMC biology qPCR array was used to determine the effects of various doses of SNP on the gene expression profiles of functionally grouped SMC markers. The fold changes in the relative gene expression of various SMC markers (a), SMC phenotypic switch markers (b), and ECM synthesis markers (c) were analyzed by the $\Delta\Delta$ Ct method. Bar graphs above the baseline value (represented by the line at y=0) represents upregulation and below the baseline represents downregulation. qPCR, quantitative polymerase chain reaction; SMC, smooth muscle cell.



obtained from the ELISA showed significant upregulation at 100 and 500 nM of SNP (p=0.03 and p=0.04 vs. control) in our Dunnett's *post hoc* analysis (Fig. 5d).

Effect of SNP on MAPK proteins

The human MAPK phosphorylation antibody array experiment results are indicated in the heat map shown in Figure 6a. The heat map indicates increased expression of MAPK signaling proteins when treated solely with cytokines (TNF α and IL-1 β). In all cases, the peak expression of these MAPKs occurred at 15 min and 30 min of cytokine exposure. Such upregulation was inhibited by the administration of 100 nM of SNP together with cytokine expo-

sure, as shown by the decreased expression of these MAPKs (Fig. 6b). The expression of JNK, ERK, AKT, MEK, MKK3, MKK6, and mTor were all inhibited by $100\,\text{nM}$ of SNP at all tested exposure times. In addition, GSK-3 (GSK3 α and GSK3 β), RSK1/2, and the transcription factor, CREB expression also decreased with SNP treatment.

Effect of SNP and NO scavenger on MAPK proteins

To further verify the role of SNP in regulating MAPKs (most specifically JNK, ERK, p-JNK, and p-ERK as these are abundantly expressed in AAAs) and to demonstrate that NO is the key regulator of this phenomenon, we performed IF-based labeling of these proteins in our cytokine-injured

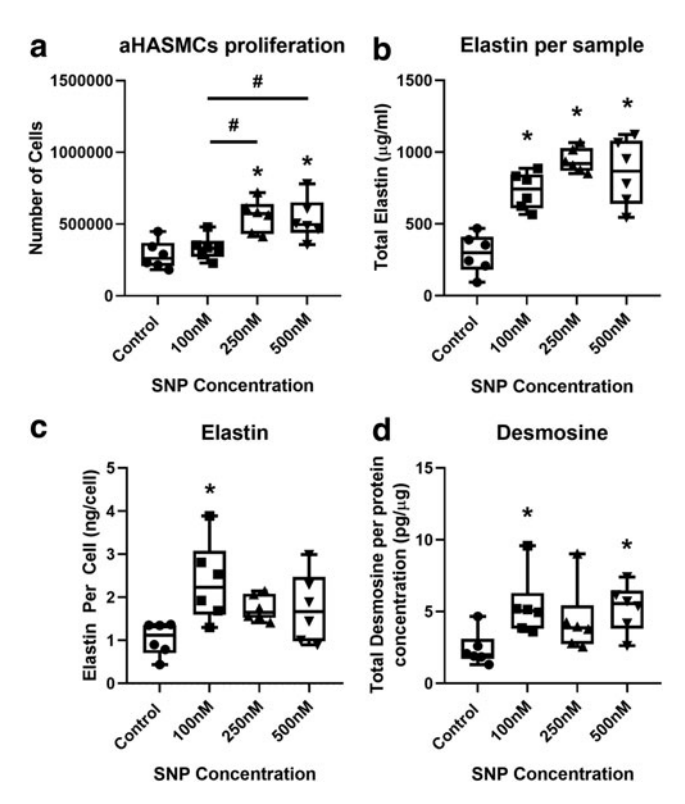


FIG. 5. The effects of SNP dose escalation, beyond the basal efficacious dose (100 nM), on aHASMC proliferation, elastic matrix synthesis, and crosslinking was shown. The effect of various SNP doses on cell proliferation (a), total elastic matrix synthesis (b), elastin amounts normalized per cell (c), and desmosine crosslinker amounts normalized to total protein (d) were quantified from various assays and represented as mean \pm SD (n=6 cultures/condition). The differences deemed statistically significant (p<0.05) compared with controls and 100 nM dose were indicated by * and #, respectively.

aHASMC cultures without and with SNP treatment (100 nM), the latter with and without an NO scavenger, PTIO (Fig. 7), for 15 min. Our IF results were consistent with our MAPK array results indicating cytokine treatment (10 ng/mL of TNF α and 10 ng/mL of IL-1 β) caused a significant upregulation in ERK and p-JNK (p<0.01) compared with control aHASMCs (without cytokine exposure) (Fig. 7b). Although expression levels of JNK and p-ERK were not significant with cytokine exposure, an increasing trend in the expression levels was still observed when exposed to cytokines. The parallel exposure of these cytokine-injured aHASMCs with 100 nM of SNP for 15 min significantly inhibited the expression of ERK (p=0.002), p-ERK (p=0.02), JNK (p=0.001), and p-JNK (p=0.04).

Conversely, the addition of $200 \, \text{nM}$ PTIO, a NO scavenger, overturned the inhibitory effect of SNP significantly on JNK (p = 0.006), p-JNK (p = 0.03), and restored their expression levels to control values or in between control and cytokine-treated values. Also, the trend in the increase or decrease of these MAPKs with cytokine treatment and with the introduction of SNP and PTIO was similar in all proteins despite their significant differences or no-significant changes among the groups. In addition, the increase or decrease

in the MMP2 expression in our IF experiment (Fig. 7a, b) can be correlated to the expression of these MAPKs, which suggests that the inhibitory effect of MMP2 was likely through the inhibition of MAPKs and was governed by released NO.

Effect of SNP on the aHASMC mechanical characteristics

Single-cell nanoindentation measurements were obtained to quantify the biophysical and biomechanical characteristics of live human aHASMCs under different SNP dosage culture conditions. The SNP dosages selected were based on cell survival and IC₅₀ studies discussed earlier. The modulus of elasticity (E_Y) decreased significantly at 10 and 100 nM exposure compared with control or 1 nM SNP dose (Fig. 8a; p < 0.05 for 10 nM vs. 100 nM). The average E_Y in control cultures was 20.9 ± 7.7 kPa and exposure to 100 nM SNP reduced it by $\sim 60\%$ to 9.64 ± 4.1 kPa.

Similarly, the forces of adhesion were not significant at 1 nM SNP versus control but were significantly reduced at 10 and 100 nM SNP (Fig. 8b; p < 0.05 for 10 nM vs. 100 nM and vs. control). The baseline adhesive forces in control cultures were 1.87 ± 0.13 nN. The tether forces (F_T) on the cell surface were significantly reduced with the addition of SNP (p < 0.05 vs. controls), even at as low as 1 nM concentration (Fig. 8c). The baseline tether forces for control cultures were 218.8 ± 14.3 pN, whereas that in the presence of 100 nM SNP dropped to 75.8 ± 12.6 pN ($\sim 65\%$ drop vs. controls).

The membrane tension and tether radius were calculated from the tether forces and trends were along expected lines as in F_T . With increasing SNP concentration, membrane tension decreased significantly (Fig. 8d) while the tether radius proportionately increased (Fig. 8e), compared with controls. The baseline membrane tension in control cultures was $6.07\pm0.8\,$ nN/ μ m, while the tether radius was $2.91\pm0.19\,$ nm. Cell roughness measurements showed that the cell surface of aHASMCs turned significantly rougher with the addition of $100\,$ nM SNP, while lower SNP dosages had no significant effect compared with controls (Fig. 8f). For all the measured parameters, no significant changes were noted at longer culture durations (24 or 48 h) in control aHASMC cultures without SNP.

Effect of SNP on the expression of ECM homeostasis proteins as seen in IF

Representative IF staining of aHASMCs for expression of MMP2, TIMP1, TIMP2, TIMP4 and ELN, LOX, and FBN1 are shown in Supplementary Figure S4. MMP2 expression in cultures treated with SNP (100 nM) was significantly suppressed relative to control cultures ($p\!=\!0.03$) and was seen as a diffused band surrounding the nuclei. SNP did not necessarily affect TIMP1 expression. However, TIMP2 and TIMP4 were found to be significantly higher in SNP-treated aHASMCs ($p\!=\!0.001$) and were seen to be expressed in a diffused manner around the cell nuclei, similar to MMP2. ELN and LOX expressions were also significantly higher in SNP-treated cultures versus controls ($p\!=\!0.004$). There were no apparent differences in FBN1 expression between control- and SNP-treated cultures.

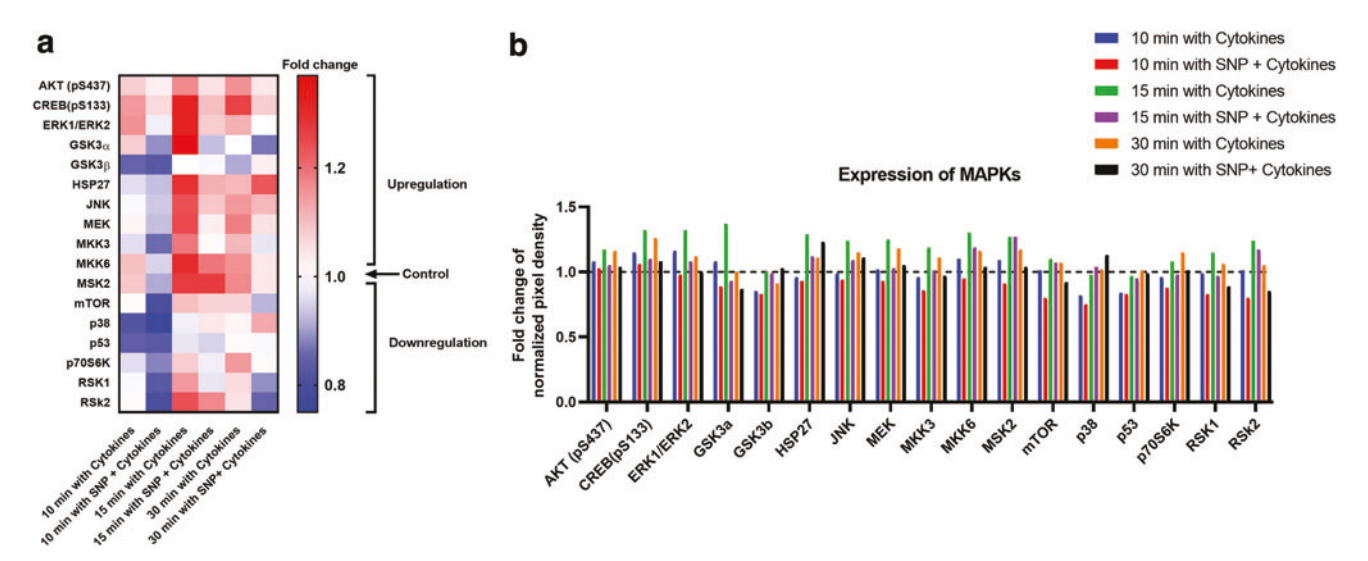


FIG. 6. Expression of phosphorylated MAPKs as a function of time in cytokine-injured aHASMC cultures with or without SNP treatment. (a) A heat map of the results from a human MAPK phosphorylation array experiment. The *red* color represents higher MAPK expression (upregulation), *blue* represents lower MAPK expression (downregulation), while *white* (indicated at 1 in the heat map) is the normalized expression of MAPKs in control cultures. Cultures received cytokine alone or cytokines and SNP for various durations, while control cultures received none. (b) Representative bar graph of the human MAPK phosphorylation experiment (n=2 repeats per condition). The mean pixel density of each target protein was normalized to the pixel density of the positive control. The *y*-axis in the graph represents the fold change obtained by normalizing the normalized pixel density to that in controls. The *dotted line* marked along y=1 represents the fold change of the untread aHASMC controls (no cytokines, no SNP). CREB, cAMP response element-binding protein; ERK, extracellular signal-regulated kinase; GSK3, glycogen-synthase kinase 3; HSP27, heat shock protein 27; JNK, c-Jun N-terminal kinase; MEK/MKK, mitogen-activated protein kinase kinase; MSK, mitogen and stress-activated kinase; mTOR, mechanistic target of rapamycin; RSK, ribosomal S6 kinase. Color images are available online.

SNP effects on elastic matrix ultrastructure as seen in TEM

TEM images showed evidence of a dense elastic matrix composed of newly formed, mature elastic fibers (black arrows) in the 100 nM SNP-treated group (Fig. 9a). In contrast, control aHASMC cultures exhibited very few, aberrant/fragmented elastic fibers (red arrow; Fig. 9b).

Discussion

AAAs represent localized expansions of the abdominal aorta due to naturally irreversible degradation and loss of wall elastic matrix caused by chronically activated MMPs following initial injury stimuli. AAA pathophysiology is exacerbated by intrinsic abnormalities in elastic fiber neoassembly and repair, chronic inflammatory response, the switch of medial SMCs to a diseased phenotype, and the association of NO signaling dysfunction. In this study, we have sought to assess if delivery of SNP (NO donor drug) is a useful treatment modality to augment elastic matrix regenerative repair and antiproteolytic effects and to promote SMC phenotypes capable of directing elastic matrix regeneration. We investigated these aspects in a cytokine injury model of human aneurysmal SMCs or aHASMCs. Proinflammatory cytokines, such as TNF α and IL-1 β , which regulate various inflammatory signaling in the cells, are known to be upregulated in AAA milieu.¹⁹

In our study, the cytokine injury model (exposure of aHASMCs to a cocktail of 10 ng/mL of TNF α and 10 ng/mL of IL-1 β) was adopted to (i) mimic and exacerbate the activated diseased state in culture following isolation from

the diseased tissue and (ii) to determine how effective SNP treatment would be in terms of elastic matrix regenerative repair under these disease-mimicking conditions. Our results indicate that 3 h of cytokine exposure has a maximal effect on aHASMCs' MMP2 production, which is the key to ECM degradation.

Next, to establish a safe, working SNP dose range, the IC₅₀ (the half maximal inhibitory concentration of SNP on cell survival) in aHASMC cultures was measured in 2% v/v FBS (low serum) and 10% v/v FBS (higher serum)containing medium. The far lower IC50 value observed in the high-serum (5.4 µM) compared with low-serum conditions (0.3 mM) (Supplementary Fig. S2) is likely due to the increased generation of reactive oxygen species (ROS) under higher serum conditions, which consequently causes more DNA damage and cell death. ^{20,21} On the other hand, SNP, at higher concentrations activates MAPKs, such as p38, through cGMP-independent pathway, which further triggers proinflammatory activation of the MMPs.²² That said, in our working SNP dose range identified based on the IC₅₀ value at high-serum conditions, overall cytotoxic effects were rather limited (<15% cell death; Supplementary Fig. S2).

Although SNP, which is an FDA-approved hypertensive drug commonly known as Nitropress[™], can activate stress-induced MAPK pathways and be associated with cyanide and ROS toxicity, our data suggest that in the working dose range in the high-serum condition, SNP likely has the anti-MAPK effect and low cyanide-related cytotoxicity. The reduced-cytotoxicity effect of SNP was further verified by our LIVE/DEAD assay results, which showed that cell death

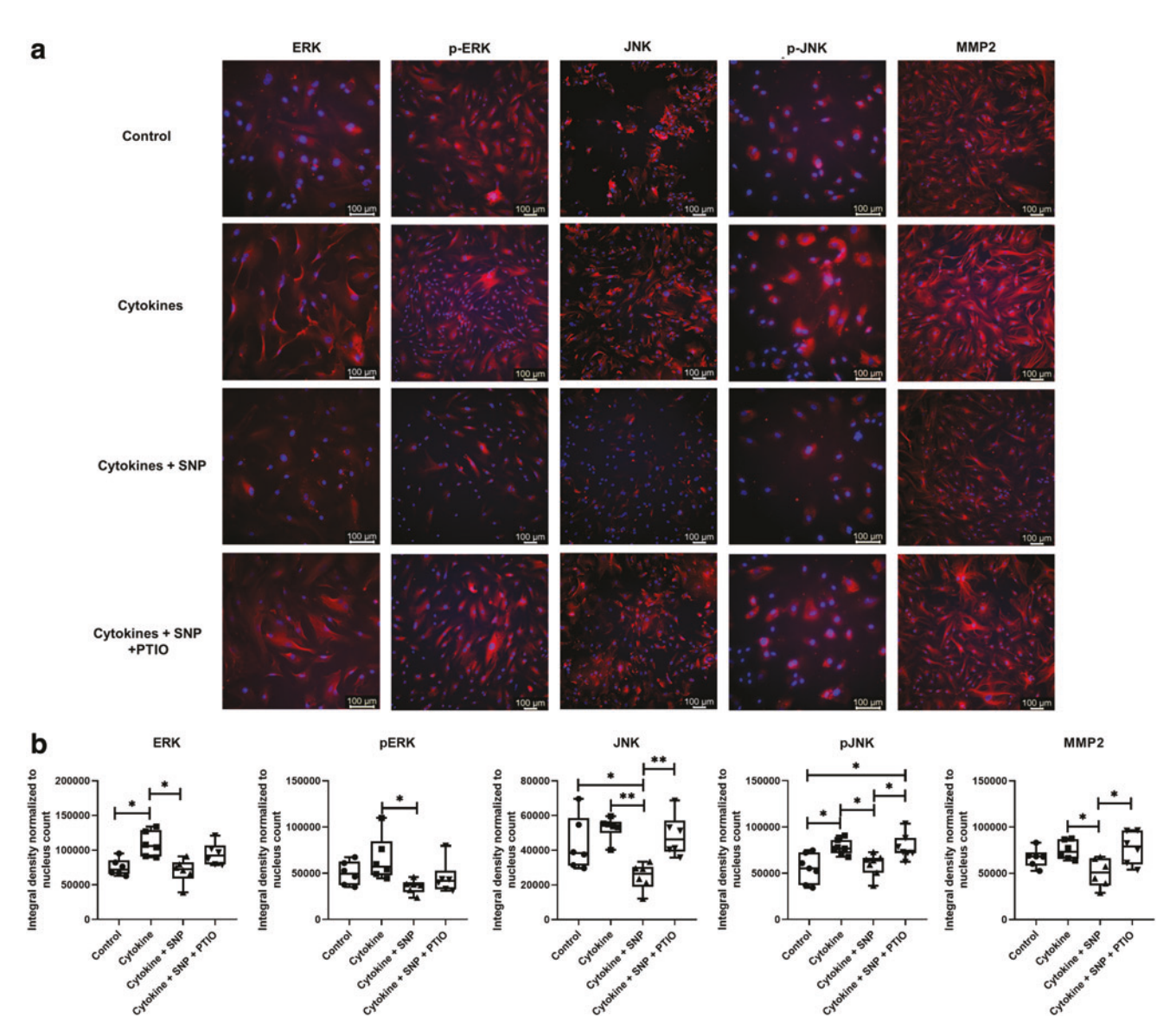


FIG. 7. IF-based demonstration of the involvement of NO in inhibiting nonphosphorylated and phosphorylated MAPKs. (a) Shows the IF-based labeling of ERK, p-ERK, JNK, p-JNK, and MMP2 in cytokine-injured, cytokine and SNP-treated, and cytokine, SNP, and PTIO (NO scavenger)-treated aHASMCs. (b) Shows the representative integral density boxplots of the respective IF images. Scale bar = $100 \, \mu m$. Data are presented as mean \pm SD of values obtained from n = 6 cultures/condition *Denotes (p < 0.05), **denotes (p < 0.05). NO, nitric oxide; PTIO, 2-phenyl-4,4,5,5-tetramethylimidazoline-1-oxyl 3-oxide. Color images are available online.

was not enhanced even at an escalated dose range of $1\,\mu M$ and $100{-}500\,n M$ (Supplementary Fig. S3). However, toxicity profiles of SNP at various serum levels should be thoroughly assessed to shed more light on SNP-induced in vitro cytotoxicity. Since low-serum condition is not physiologically relevant, to reflect in vivo conditions more closely, we adopted higher serum conditions for in vitro assessment.

Next, we investigated the effects of SNP on the expression of ECM homeostasis proteins in our cultures. Several *in vitro* studies have suggested a possible connection between NO deficiency and chronic overexpression of the elastolytic MMPs (MMP2 and MMP9), the most abundant endopeptidases in the AAA wall, which critically drive elastic matrix degradation. ^{23,24} To date, a spate of published studies has also demonstrated that inhibiting MMP2 and

MMP9 can attenuate inflammatory tissue damage following injury, ²⁵ and limit chronic MMP-mediated ECM breakdown and loss. ²⁶ Consistent with earlier findings, our results showed SNP delivery to significantly downregulate MMP2 expression (Figs. 2b and 3a and Supplementary Fig. S4a, b) and MMP2 enzyme activity (Fig. 3g). MMP2 expression in treated aHASMCs (Figs. 1a and 7a and Supplementary Fig. S4), as seen in our IF images, shows diffused and spread patterns, which is consistent with results of another published study. ²⁷

The lack of any discernable effects on MMP9 expression (data not shown), despite the evidence of NO-mediated MMP9 inhibition in human umbilical vein endothelial cells and rat mesangial cells, ^{28,29} is likely due to a very low intrinsic expression of MMP9 (protein and gene) in cell culture, which is likely because of the absence of macrophages

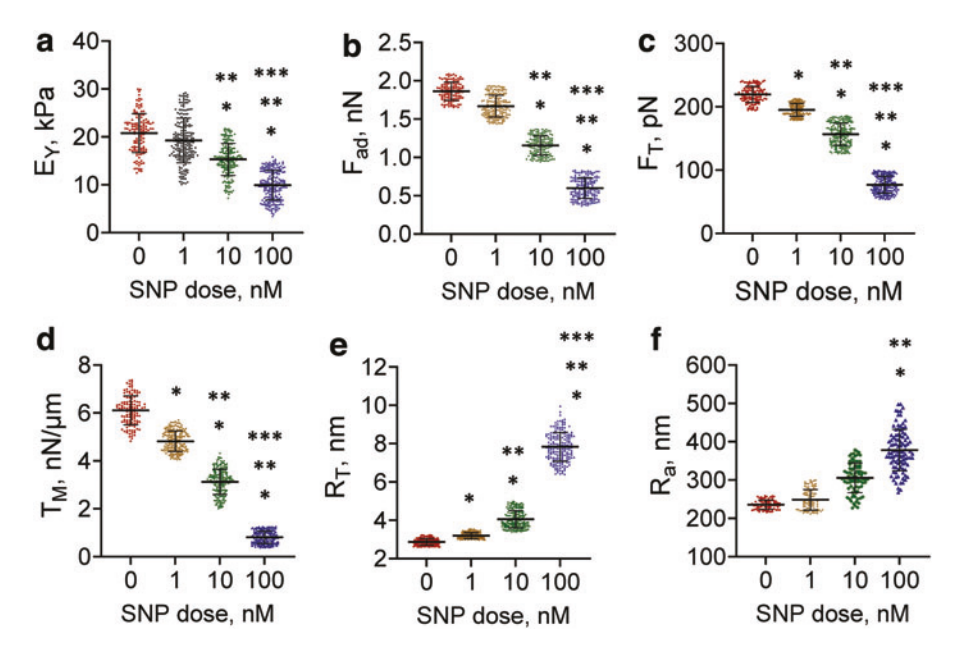


FIG. 8. Dose-dependent effect of higher SNP doses (1, 10, 100 nM) on cellular elastic response as determined by AFM. (a) Elastic modulus of the cells (E_Y) calculated by applying Hertz model to force-indentation curves ($128 \le n \le 205$ cells/condition). (b) Adhesion forces measured from the force-indentation curves during retraction mode ($109 \le n \le 167$ cells/condition). (c) Tether forces measured from the force-indentation curves during retraction mode ($119 \le n \le 188$ cells/condition). (d) Membrane tension on the cell surface (T_M) calculated from the tether forces using $T_M = F_T^2/8\pi^2k_B$. (e) The radius of tether (R_T) calculated from F_T values using $R_T = 2\pi k_B/F_T$. (f) The surface roughness parameter (R_a) on the cell surface measured using AFM tip ($77 \le n \le 98$ cells/condition) for control and SNP-exposed cells. Data were presented as mean \pm SD, with statistical significance deemed for p < 0.05 and indicated by * for differences versus control, ** for differences versus 1 nM dose of SNP, and *** for differences versus 10 nM dose of SNP. AFM, atomic force microscopy. Color images are available online.

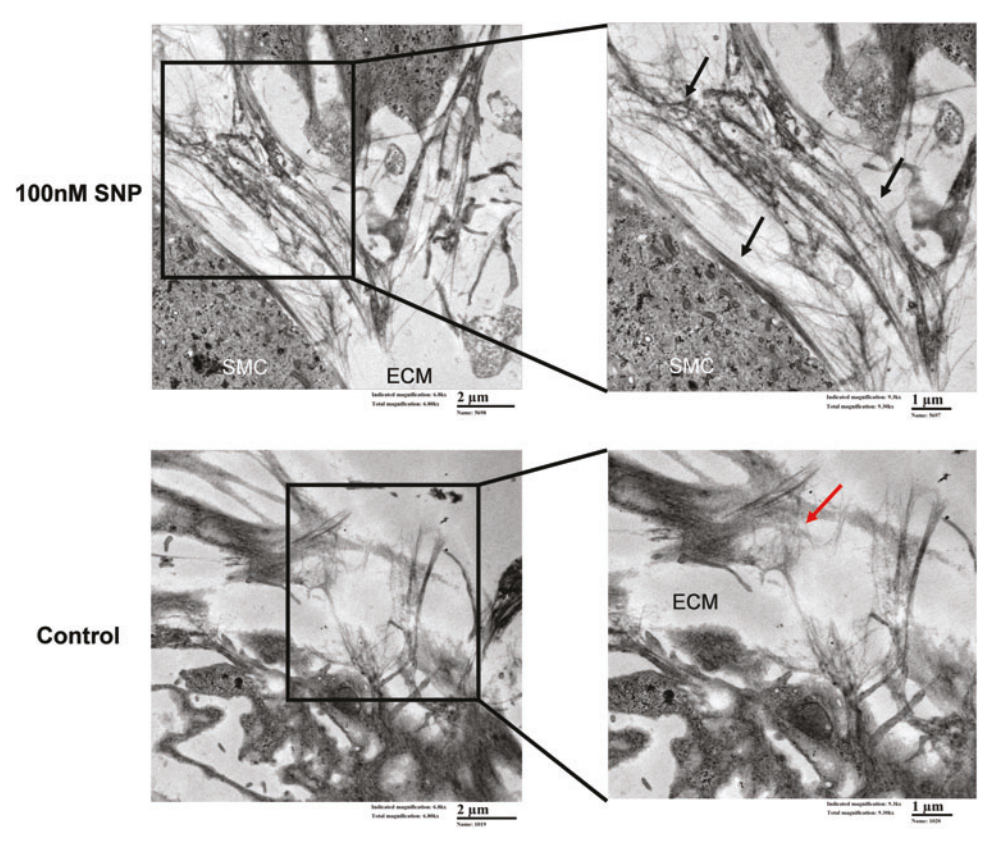


FIG. 9. The effect of SNP treatment on elastic matrix ultrastructure formed in cell cultures was imaged using transmission electron microscopy. (a) Ultrastructure of thick, newly formed, elastic fibers composed of elastin coacervates (tropoelastin) shown in black arrow in 100 nM SNP-treated aHASMC cultures after 14 days of exposure. (b) Thin and fragmented elastin-associated structures in untreated control group (red arrow). Color images are available online.

and macrophage-generated reactive nitrogen oxide species linked to triggering MMP9 activation. ²⁸ As a next step, we propose to investigate possible SNP effects on MMP9 in a more complex *in vitro* culture model incorporating matrix debridement with macrophages, which we have published. ³⁰

Our results further indicate that the inhibition of MMP2 can be linked to the significant increase in TIMP2 and TIMP4 (inhibitors of MMPs) (Fig. 2b and Supplementary Fig. S4a, b). However, no significant change was seen in TIMP4 WBs, but, it colocalized with active MMP2 bands (Fig. 3b) suggesting the potential inhibitory effect of TIMP4 against MMP-mediated proteolysis likely by fine-tuning active-MMP activities as suggested by few studies. 31,32

Despite the substantial increase in TIMP2 gene and protein expression with both RT-PCR and IF at 100nM of SNP, we were unable to detect TIMP2 with WB while TIMP1 expression did not change in RT-PCR (Fig. 2b) and in IF (Supplementary Fig. S4a, b) and remained undetected in WB like TIMP2. This outcome is likely due to the inherent difference in the probe sensitivity and binding efficiency of TIMP1 and TIMP2 to their respective antibodies, and low protein yield from our cultures, which limited protein loading onto our WB gels. In terms of gene expression ratio, there was a significant increase in TIMP1 to MMP2 and TIMP2 to MMP2 ratio showing the potential anti-MMP effect of SNP (at 100 nM) in our aHASMC cultures (Fig. 2d).

The anti-MMP effect of SNP we observed can involve activation of either cGMP-dependent pathways, cGMPindependent pathways, or both by the NO released from SNP.^{4,5} While the primary focus of this study lies in assessing SNP effects in promoting elastin homeostasis in the context of AAAs, we have sought to broadly understand the underlying mechanisms, specifically the involvement of the cGMP-independent pathway. This pathway regulates various cellular transcription factors and consequently modulates gene and protein expressions of the cells through S-nitrosylation of cysteine residues of the receptors of the MAPK pathways.³³ Among several MAPKs, the JNK and ERK signaling pathways have been most implicated in AAAs.^{8,34} Our findings suggest significant downregulation in ERK1 and ERK2 gene expressions (Fig. 2c), but no difference in gene and protein expression of other MAPKs, for example, JNK1 and JNK2 with SNP treatment. This is probably due to the transient expression of these MAPK proteins and their relatively shorter half-life, which renders their detection in long-term-treated (7 days) cultures challenging.³⁵

Therefore, to further demonstrate the role of SNP in regulating transiently expressed MAPKs, we performed a MAPK array experiment at short cytokine and SNP exposure times (<30 min) in our culture model. This MAPK array provides the screening of a broader spectrum of MAPKs, which likely has a direct or indirect association with the inflammatory milieu of proteolytic disorders, such as in AAAs.

Most of the MAPKs, such as AKT, CREB, ERK1, ERK2, JNK, MEK, MKK3, MKK6, MSK2, mTor, p38, p53, RSK1, and RSK2, are implicated in proteolytic disorders, with JNK and ERK being the primary MAPKs that drives the formation and progression of AAAs.^{34–37} While our WB result showed no significant differences in JNK and ERK expression at a 7-day time point, downregulation of these MAPKs was observed in the MAPK array experiments at time points of 0–30 min (Fig. 6). To further verify the role of cytokine

and SNP exposure in downregulating MAPKs (specifically JNK, p-JNK, ERK, and p-ERK) and to determine if these effects were mediated by NO released from SNP, we performed IF-based labeling of these MAPKs, which showed significant upregulation and downregulation of MAPKs with cytokine exposure and with parallel SNP treatment, respectively (Fig. 7a, b). However, this effect was completely overturned with the addition of NO scavenger, PTIO, which suggests that the SNP-mediated MAPK inhibition was regulated by NO.

In addition, the expression of MMP2 showed positive correlation to MAPK expression, which suggests that the anti-MMP effect in our aHASMC cultures is linked to MAPK attenuation. Moreover, SNP treatment caused the downregulation of other MAPKs as seen in our MAPK array results. GSK-3 is considered to be at the crossroads of various other signaling pathways, including EGFR, Ras, AKT, and mTor, and is known to control Nf-κβ activity through IkappaB kinase/Nf-κβ essential modifier regulation. 38,39 Similarly, CREB is a transcription factor that regulates various gene expressions in response to the cAMP changes and has also been shown to regulate expressions of MMP 2 in other cell types. 40 Other isoforms of MAPKs, such as MEK, MKK3, MKK6, MSK2, p38, p53, RSK1, and RSK2, also control a wide range of biological functions and therefore increase the range of action regulated by the active forms of MAPKs mentioned above to drive the inflammatory response.41

Overall, our MAPK array experiment has demonstrated that SNP has inhibitory effects on various MAPKs, which perhaps occurs through disorganization of actin filaments possibly through cGMP-dependent signaling and/or by attenuation of NOTCH signaling pathway. NOTCH signaling pathways have been previously shown to specifically activate the MEK, ERK, and AKT pathways. On this basis, we hypothesize that the SNP-mediated MAPK inhibition in our study is mediated by disruption of the actin cytoskeleton (Figs. 2a and 3a) and *NOTCH* deactivation (Fig. 4b).

Also, NOTCH signaling is associated with the phenotypic modulation of VSMCs. 2,46,47 Increased activity of NOTCH1 and NOTCH3 have been shown to promote SMCs proliferation, and collagen synthesis, and induce a synthetic SMC phenotype through downstream regulation of CHF1/HEY2. 48 Downregulation of HEY2, NOTCH1, and NOTCH3 in our qPCR array (Fig. 4b) and our experimental findings on cell proliferation particularly at 100 nM SNP (Fig. 5a) suggest that the cells are not assuming a highly synthetic SMC phenotype that could potentially promote hyperplasia in a AAA wall milieu.

This is also supported by our RT-PCR results showing unchanged expression of end-stage SMC contractile phenotypic markers (*SMTH* and *CNN*; Fig. 2a) between SNP-treated and untreated groups. The decrease in *COL3A1* gene expression (Fig. 2c) in RT-PCR and lower expressions of collagens in the qPCR array (Fig. 2c), whose expression is elevated in SMCs of a synthetic SMC phenotype, ⁴⁹ also supports the inference that SNP exposure does not trigger a highly synthetic SMC phenotype. On the other hand, as anticipated, there was a significant downregulation in *ACTA*, *DES*, and *MYH11* (Fig. 2a) genes encoding contractile apparatus proteins as NO donor compounds have been frequently shown to downregulate contractile

apparatus genes and induce muscle relaxation by down-regulating interactions of the actin–tropomyosin–myosin complex involved in the sliding filament mechanism of cell contraction. ^{50,51} Collectively, our gene expression analysis and biochemical assay results indicate that at 100 nM, SNP did not induce synthetic phenotypes in culture but did promote a more relaxed cell state.

To investigate the phenotypic changes in aHASMCs in response to NO exposure, we performed AFM analysis. We sought to address two primary questions: (i) if NO exposure softens the cells, and if so, the dose dependency of this effect, and (ii) if NO exposure causes any change to the cell surface? Live cell indentation of aHASMCs with AFM (Fig. 8) showed a significant reduction of Young's modulus and cell surface adhesive forces at SNP doses of 10 and 100 nM suggesting aHASMCs acquired softer characteristics with SNP treatment. Similarly, tether force, which is dependent on membrane adhesion as well as cytoskeleton adhesion was significantly reduced with increasing SNP dosage in our study suggesting decreased cytoskeletal density in the aHASMC cultures. 52 The decreased gene expression of ACTA, MYH11, and DES in our gene study further verifies that the decrease in these forces is likely because of a decrease in the cytoskeletal protein expression with SNP treatment.53

Furthermore, the radius of tether and surface roughness increased with increasing SNP concentrations, possibly through a similar mechanism explained above and through modulation of cell surface proteins.⁵⁴ Overall, our study showed that the forces required to separate the nonfunctionalized polystyrene bead-modified AFM tip from the cell surface were strongly dependent on the SNP concentration in the culture media. aHASMCs turned softer from a stiffness standpoint, while their surfaces turned pliable and rough in the presence of SNP similar to what was noted in prior study.⁵⁴ The no significant change in the control cultures at longer time points verifies that the differences seen in these parameters were mediated by SNP. In addition, the glycocalyx might also be undergoing some changes in response to NO exposure, as shown by the decreased adhesion force, although such changes are tedious to quantify using other techniques.

In healthy vessels, the turnover of structural ECM proteins (e.g., elastin and collagen) is very low due to low MMP activity and an intrinsic balance between MMPs and TIMPs. Differently, the chronic upregulation of MMPs in the AAA wall leads to increased fragmentation of both elastic fibers and collagen fibers to cause ultimate wall weakening and rupture.⁵⁵ Elastic matrix regeneration is particularly challenging due to the poor intrinsic elastin synthesis capacity of adult and diseased VSMCs and their impaired ability to assemble mature elastic fibers. Different from elastin, vascular SMCs robustly synthesize collagen, thereby increasing the collagen-to-elastin ratio either by collagen synthesis and/or disproportionate degradation of noncollagenous structural proteins.⁵⁶ Our findings demonstrate that elastic matrix synthesis by aHASMCs is significantly enhanced with SNP treatment as suggested by increased ELN gene expression at 100 nM SNP (Fig. 2b), protein expression (Supplementary Fig. S4c, d), and increases in total matrix elastin amounts and on a per-cell basis (Fig. 5b, c) at 100 nM.

Tropoelastin often appears localized within or around the cell, likely due to the fact that most of the ECM proteins are produced by SMCs in the cell or on the cell surface in their precursor form (elastin and collagen) where they begin to form crosslinks and are eventual organization into fibers in the etxracellular space and their subequent maturation.^{57,58} Due to their aberrant diseased phenotype and intrinsic deficiency in generating mature elastic fibers, our IF images primarily show tropoelastin within and adjacent to cells, with no discernable organized extracellular structures. Accordingly, to elucidate further on this, we performed TEM of our cultured aHASMCs to visualize the ultrastructure of the deposited fibers and verify if the newly formed elastic matrix is deposited in the extracellular space or within the cells. TEM images (Fig. 9) show that SNP treatment stimulated formation of elastic fibers, still in the process of maturation, and the majority of which was deposited along the cell membrane and adjaced extracellular space. In contrast, the untreated control cultures contained few, if at all any evidence of frustrated elastic fiber assembly.

While collagen protein amounts were below the threshold for reliable detection, the significant increases seen in the ELN/COL3A1 ratio (Fig. 2d) at the proelastogenic/ antiproteolytic SNP dose (100 nM) suggests progress toward restoring ECM homeostasis with SNP treatment as collagen accumulation is primarily associated with an adverse fibrotic response of vascular SMCs and contribute to the vascular stiffness.⁵⁹ A possible reason for having no detected collagen in our cultures is likely because (i) fibroblasts and not SMCs are the primary source of collagen in the aorta wall, and (ii) our aHASMCs, having been isolated from rupture stage AAA tissues exhibit a highly diseased phenotype characterized by poor ECM production; at the later stages of AAA progression when an aneurysm reaches a ruptureprone stage, chronic proteolytic degradation of both collagen and elastin occurs and the cells gradually lose their ability to restore these elastic matrix assembly and other extracellular proteins.⁵⁵

Moreover, a published study has shown that SNP treatment in vascular SMC inhibits collagen production by 42%, 60 which might also explain the reason for below-threshold collagen levels in our aHASMC cultures treated with SNP. Furthermore, the coacervation and crosslinking of elastin precursors by LOX provide structural integrity to the ECM by forming strong intermolecular covalent bonds between elastin precursors. 61

LOX (precursor, 50 kDa) produced by SMCs are hydrolyzed into their active form that promotes crosslinking of fibrous ECM proteins, such as elastin and collagen, into a nonsoluble state. The inactivation of the *LOX* gene resulted in the formation of large aortic aneurysms, cardiovascular dysfunction, and perinatal death in LOX knockout (LOX^{-/-}) mice. Conversely, an increase in LOX has been shown to improve elastic matrix crosslinking. Consistent with these outcomes, our observed increases in the *LOX* gene (Fig. 2b) and LOX protein expression (Fig. 3f and Supplementary Fig. S4c, d) with SNP treatment correlated positively with increased expression of desmosine (Fig. 5d). Desmosine is a crosslinker molecule essential for elastic matrix formation, crosslinking, and maturation.

The formation of desmosine occurs within the formation of precursor tropoelastin. During development, SMCs

produce tropoelastin on the cell surface where LOX helps in the oxidative deamination of lysine residues of tropoelastin to form allysine that further reacts with other lysine residues of tropoelastins to form desmosine. ^{57,64} Our observed increases in desmosine content with SNP treatment of cultures can be inferred to be indicative of increased crosslinking of the elastin. Additionally, once the crosslinking process of many soluble elastin precursors is done, the elastic matrix is finally deposited on the ECM for further maturation and crosslinking. ⁶⁵

Elastic fiber assembly is a complex, multistep process orchestrated by several key proteins and glycoproteins. Fibulins (FBLNs), particularly Fibulin 4 and 5, facilitate crosslinking of tropoelastin to form coacervates that engage with a prescaffold of FBN1 glycoprotein to promote elastic fiber assembly. ⁶⁶ However, despite SNP-induced increases in elastin and LOX, in the tested dose range, SNP did not impact gene and protein expression of FBLNs (data not

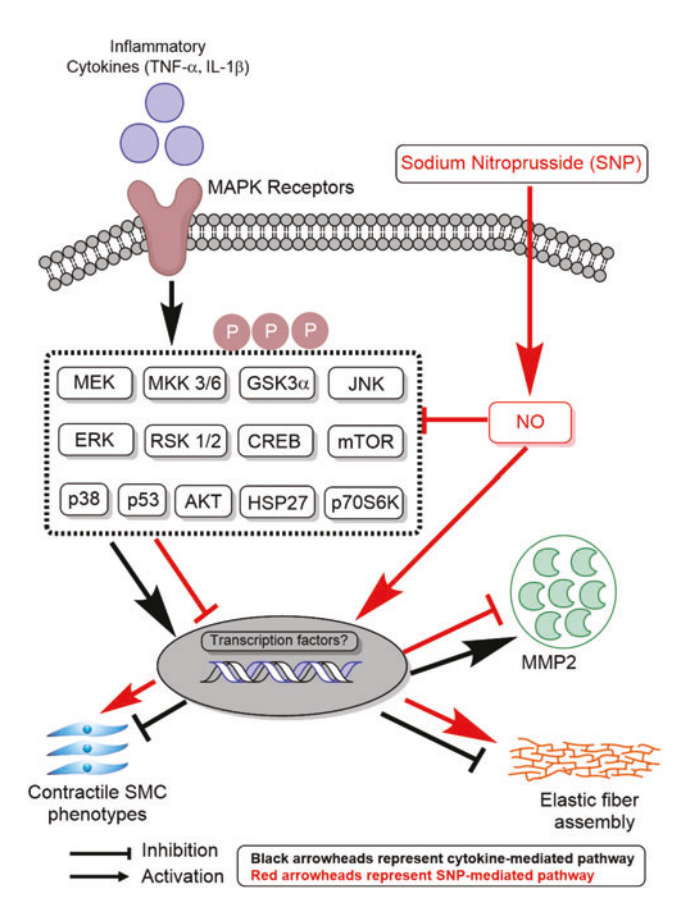


FIG. 10. Suggested MAPK-mediated mechanistic pathway engaged by SNP for antiproteolytic and proelastogenic regulation of ECM homeostasis in aHASMCs. *Arrows* indicate activation and T lines represent inhibition. Question mark indicate that the critical transcription factors are remained to be identified. Inflammatory cytokines (TNFα and IL-1β) activated MAPK signaling. SNP attenuated these MAPKs to or below the control value, which in turn attenuated MMP2 (gene and protein expression), increased elastic matrix components (elastin, LOX, desmosine), and promoted contractile SMC phenotypes. IL-1β, interleukin-1 beta; LOX, lysyl oxidase; TNFα, tumor necrosis factoralpha. Color images are available online.

shown) and FBN1 (Figs. 2c and 3e and Supplementary Fig. S4c, d). Despite this, our TEM experiment shows evidence of elastic fiber assembly in aHASMC cultures treated with 100 nM SNP (Fig. 9), broadly consistent with the ultrastructure shown by Robb et al,⁶⁷ while sporadic and thin elastin-associated structures were seen in the untreated controls. Based on our above findings, we deduce that these outcome are driven primarily by increases in tropoelastin synthesis, and desmosine and LOX-mediated crosslinking rather than by increases in assessed elastic fiber assembly proteins, such as fibrillin and fibulins.

In addition to the improvement in the elastic matrix assembly in aHASMCs with SNP treatment, various studies have reported that SNP increases compliance of the aortic wall consequently decreasing the arterial stiffness and providing mechanical stability to the aortic stretch and recoil function. As collagen is the major determinant of matrix stiffness, the decreased expression of collagen genes, no detection of collagen in our biochemical assays, upregulation of elastin to collagen gene expression ratio, and upregulation of elastic matrix deposition and crosslinking suggest that SNP treatment does not probably contribute to ECM stiffness, rather, it might improve the elastic function of the ECM. Since microcalcification of the arterial wall is related to arterial stiffness, and SNP suppresses calcification by decreasing calcium current in the cells, it is expected that SNP likely reduces calcification of the vessel wall

However, to determine how SNP contributes to the long-term stabilization of the mechanical properties of the ECM, more extensive studies in *in vitro* (3D) cultures and *in vivo* studies might be required. In a nutshell, the antiproteolytic and proelastogenic effects of SNP as seen in our *in vitro* study are summarized in Figure 10.

Conclusions

This study has demonstrated that SNP treatment is useful to restore ECM homeostasis and modulate the phenotype of human aneurysmal SMC in vitro cultures. SNP upregulated elastic matrix assembly, crosslinking, and maturation and concurrently inhibited MMPs through NO-mediated MAPK inhibition. In addition to this, we have also demonstrated the ability of SNP to promote contractile subpopulations of SMCs in culture conditions, which promote elastic matrix synthesis. However, one potential drawback of exogenous SNP delivery is that NO is immediately released in the aqueous microenvironment and being a short-lived molecule, quickly oxidizes into less effective nitrite and nitrate in aqueous conditions. Our future work will thus focus on the controlled delivery of SNP encapsulated within nanocarriers, which will also offer opportunities for localized drug delivery at efficacious doses within the AAA wall in vivo. The proposed approach has the potential to delay the growth of small AAAs to a rupture stage that mandates risky surgery for mostly older AAA patients.

Acknowledgment

The authors would like to acknowledge Ms. Mei Yin at the Electron Microscopy Core of the Lerner Research Institute, Cleveland Clinic for her assistance with TEM imaging.

Authors' Contributions

S.B.: conception and design of all experiments, data collection and/or data assembly, data analysis and interpretation, and article writing. C.K.: data collection, analysis, and interpretation of AFM experiment, and article writing. A.R.: conception and design of all experiments, data collection and/or data assembly, data analysis and interpretation, and article writing. All authors read an approved the final article.

Disclosure Statement

No competing financial interests exist.

Funding Information

This research was supported by the American Heart Association (AHA) (Grant No. 19TPA34890029), National Institute of Health (NIH) (Grant No. HL139662), the National Science Foundation (NSF) (Grant No. 1926939) awarded to Anand Ramamurthi, and the NSF grant (Grant No. 1927602) awarded to Chandrasekhar Kothapalli.

Supplementary Material

Supplementary Table S1

Supplementary Figure S1

Supplementary Figure S2

Supplementary Figure S3

Supplementary Figure S4

References

- Kuivaniemi H, Ryer EJ, Elmore JR, et al. Understanding the pathogenesis of abdominal aortic aneurysms. Expert Rev Cardiovasc Ther 2015;13(9):975–987; doi: 10.1586/ 14779072.2015.1074861
- Lu H, Du W, Ren L, et al. Vascular smooth muscle cells in aortic aneurysm: From genetics to mechanisms. J Am Heart Assoc 2021;10(24):e023601; doi: 10.1161/JAHA.121 .023601
- 3. Keeley FW. The synthesis of soluble and Insoluble elastin in chicken aorta as a function of development and age. Effect of a high cholesterol diet. Can J Biochem 1979; 57(11):1273–1280; doi: 10.1139/o79-169
- Cui X, Zhang J, Ma P, et al. cGMP-independent nitric oxide signaling and regulation of the cell cycle. BMC Genomics 2005;6:151; doi: 10.1186/1471-2164-6-151
- Denninger JW, Marletta MA. Guanylate cyclase and the •NO/cGMP signaling pathway. Biochim Biophys Acta 1999;1411(2):334–350; doi: 10.1016/S0005-2728(99) 00024-9
- Laaksamo E, Tulamo R, Baumann M, et al. Involvement of mitogen-activated protein kinase signaling in growth and rupture of human intracranial aneurysms. Stroke 2008; 39(3):886–892; doi: 10.1161/STROKEAHA.107.497875
- DiMusto PD, Lu G, Ghosh A, et al. Increased JNK in males compared to females in a rodent model of abdominal aortic aneurysm. J Surg Res 2012;176(2):687–695; doi: 10.1016/ j.jss.2011.11.1024
- Camardo A, Seshadri D, Broekelmann T, et al. Multifunctional, JNK-inhibiting nanotherapeutics for augmented elastic matrix regenerative repair in aortic aneurysms. Drug Deliv Transl Res 2018;8(4):964–984; doi: 10.1007/s13346-017-0419-y

- Park H-S, Huh S-H, Kim M-S, et al. Nitric oxide negatively regulates c-Jun N-terminal kinase/stress-activated protein kinase by means of S-nitrosylation. Proc Natl Acad Sci U S A 2000;97(26):14382–14387.
- Gacchina CE, Deb P, Barth JL, et al. Elastogenic inductability of smooth muscle cells from a rat model of late stage abdominal aortic aneurysms. Tissue Eng Part A 2011;17(13–14):1699–1711; doi: 10.1089/ten.tea.2010.0526
- 11. Livak KJ, Schmittgen TD. Analysis of relative gene expression data using real-time quantitative PCR and the $2-\Delta\Delta CT$ method. Methods 2001;25(4):402–408; doi: 10.1006/meth.2001.1262
- 12. Venkataraman L, Ramamurthi A. Induced elastic matrix deposition within three-dimensional collagen scaffolds. Tissue Eng Part A 2011;17(21–22):2879–2889; doi: 10.1089/ten.tea.2010.0749
- 13. Swaminathan G, Stoilov I, Broekelmann T, et al. Phenotype-based selection of bone marrow mesenchymal stem cell-derived smooth muscle cells for elastic matrix regenerative repair in abdominal aortic aneurysms. J Tissue Eng Regen Med 2018;12(1):e60–e70; doi: 10.1002/term .2349
- Labarca C, Paigen K. A simple, rapid, and sensitive DNA assay procedure. Anal Biochem 1980;102(2):344–352; doi: 10.1016/0003-2697(80)90165-7
- Stoilov I, Starcher BC, Mecham RP, et al. Measurement of elastin, collagen, and total protein levels in tissues. Methods Cell Biol 2018;143:133–146 doi: 10.1016/bs.mcb.2017 .08.008
- 16. Edwards CA, O'Brien WD. Modified assay for determination of hydroxyproline in a tissue hydrolyzate. Clin Chim Acta 1980;104(2):161–167; doi: 10.1016/0009-8981(80) 90192-8
- 17. Dudiki T, Mahajan G, Liu H, et al. Kindlin3 regulates biophysical properties and mechanics of membrane to cortex attachment. Cell Mol Life Sci 2021;78(8):4003–4018; doi: 10.1007/s00018-021-03817-7
- Dahal S, Broekelman T, Mecham RP, et al. Maintaining elastogenicity of mesenchymal stem cell-derived smooth muscle cells in two-dimensional culture. Tissue Eng Part A 2018;24(11–12):979–989; doi: 10.1089/ten.tea.2017 .0237
- Batra R, Suh MK, Carson JS, et al. IL-1β and TNF-α impact abdominal aortic aneurysm formation by differential effects on macrophage polarization. Arterioscler Thromb Vasc Biol 2018;38(2):457–463; doi: 10.1161/ATV BAHA.117.310333
- Valverde M, Lozano-Salgado J, Fortini P, et al. Hydrogen peroxide-induced DNA damage and repair through the differentiation of human adipose-derived mesenchymal stem cells. Stem Cells Int 2018;2018:1615497; doi: 10.1155/2018/1615497
- 21. Li K, Li Y, Mi J, et al. Resveratrol protects against sodium nitroprusside induced nucleus pulposus cell apoptosis by scavenging ROS. Int J Mol Med 2018;41(5):2485–2492; doi: 10.3892/ijmm.2018.3461
- 22. Rabkin SW, Klassen SS, Tsang MY. Sodium nitroprusside activates p38 mitogen activated protein kinase through a cGMP/PKG independent mechanism. Life Sci 2007;81(8): 640–646; doi: 10.1016/j.lfs.2007.06.022
- 23. Upchurch GR, Ford JW, Weiss SJ, et al. Nitric oxide inhibition increases matrix metalloproteinase–9 expression by rat aortic smooth muscle cells in vitro. J Vasc Surg 2001;34(1):76–83; doi: 10.1067/mva.2001.115598

- 24. Souza-Pinto FJP, Moretti AIS, Cury V, et al. Inducible nitric oxide synthase inhibition increases MMP-2 activity leading to imbalance between extracellular matrix deposition and degradation after polypropylene mesh implant. J Biomed Mater Res A 2013;101A(5):1379–1387; doi: 10.1002/jbm.a.34440
- 25. Kim K-H, Burkhart K, Chen P, et al. Tissue inhibitor of metalloproteinase-1 deficiency amplifies acute lung injury in bleomycin-exposed mice. Am J Respir Cell Mol Biol 2005;33(3):271–279; doi: 10.1165/rcmb.2005-0111OC
- 26. Breynaert C, de Bruyn M, Arijs I, et al. Genetic deletion of tissue inhibitor of metalloproteinase-1/TIMP-1 alters inflammation and attenuates fibrosis in dextran sodium sulphate-induced murine models of colitis. J Crohns Colitis 2016;10(11):1336–1350; doi: 10.1093/ecco-jcc/jjw101
- 27. Lee E-J, Zheng M, Craft CM, et al. Matrix metalloproteinase-9 (MMP-9) and tissue inhibitor of metalloproteinases 1 (TIMP-1) are localized in the nucleus of retinal Müller glial cells and modulated by cytokines and oxidative stress. PLoS One 2021;16(7):e0253915; doi: 10.1371/journal.pone.0253915
- 28. Phillips PG, Birnby LM. Nitric oxide modulates caveolin-1 and matrix metalloproteinase-9 expression and distribution at the endothelial cell/tumor cell interface. Am J Physiol-Lung Cell Mol Physiol 2004;286(5):L1055–L1065; doi: 10.1152/ajplung.00262.2003
- 29. Eberhardt W, Beeg T, Beck K-F, et al. Nitric oxide modulates expression of matrix metalloproteinase-9 in rat mesangial cells. Kidney Int 2000;57(1):59–69; doi: 10.1046/j.1523-1755.2000.00808.x
- 30. Gacchina C, Brothers T, Ramamurthi A. Evaluating smooth muscle cells from CaCl2-induced rat aortal expansions as a surrogate culture model for study of elastogenic induction of human aneurysmal cells. Tissue Eng Part A 2011;17(15–16):1945–1958; doi: 10.1089/ten.tea.2010.0475
- Huang B, Zhao X, Zheng L-B, et al. Different expression of tissue inhibitor of metalloproteinase family members in rat dorsal root ganglia and their changes after peripheral nerve injury. Neuroscience 2011;193:421–428; doi: 10.1016/ j.neuroscience.2011.07.031
- 32. Hernandez-Barrantes S, Shimura Y, Soloway PD, et al. Differential roles of TIMP-4 and TIMP-2 in pro-MMP-2 activation by MT1-MMP. Biochem Biophys Res Commun 2001;281(1):126–130; doi: 10.1006/bbrc.2001.4323
- 33. Ridnour LA, Windhausen AN, Isenberg JS, et al. Nitric oxide regulates matrix metalloproteinase-9 activity by guanylyl-cyclase-dependent and -independent pathways. Proc Natl Acad Sci U S A 2007;104(43):16898–16903; doi: 10.1073/pnas.0702761104
- 34. Ghosh A, DiMusto PD, Ehrlichman LK, et al. The role of extracellular signal-related kinase during abdominal aortic aneurysm formation. J Am Coll Surg 2012;215(5):668-680.e1; doi: 10.1016/j.jamcollsurg.2012.06.414
- Nguyen DHD, Hussaini IM, Gonias SL. Binding of urokinase-type plasminogen activator to its receptor in MCF-7 cells activates extracellular signal-regulated kinase 1 and 2 which is required for increased cellular motility. J Biol Chem 1998;273(14):8502–8507; doi: 10.1074/jbc.273.14.8502
- 36. Ghosh A, Lu G, Su G, et al. Phosphorylation of AKT and abdominal aortic aneurysm formation. Am J Pathol 2014; 184(1):148–158; doi: 10.1016/j.ajpath.2013.09.016
- 37. Wang Z, Guo J, Han X, et al. Metformin represses the pathophysiology of AAA by suppressing the activation of

- PI3K/AKT/mTOR/autophagy pathway in ApoE-/- mice. Cell Biosci 2019;9(1):68; doi: 10.1186/s13578-019-0332-9
- 38. Duda P, Akula SM, Abrams SL, et al. Targeting GSK3 and associated signaling pathways involved in cancer. Cells 2020;9(5):1110; doi: 10.3390/cells9051110
- Medunjanin S, Schleithoff L, Fiegehenn C, et al. GSK-3β controls NF-kappaB activity via IKKγ/NEMO. Sci Rep 2016;6:38553; doi: 10.1038/srep38553
- Salhi A, Farhadian JA, Giles KM, et al. RSK1 activation promotes invasion in nodular melanoma. Am J Pathol 2015;185(3):704–716; doi: 10.1016/j.ajpath.2014.11.021
- 41. Cargnello M, Roux PP. Activation and function of the MAPKs and their substrates, the MAPK-activated protein kinases. Microbiol Mol Biol Rev 2011;75(1):50–83; doi: 10.1128/MMBR.00031-10
- 42. Ingram AJ, James L, Cai L, et al. NO inhibits stretch-induced MAPK activity by cytoskeletal disruption. J Biol Chem 2000;275(51):40301–40306; doi: 10.1074/jbc.M00 7018200
- 43. Kim M-Y, Park J-H, Mo J-S, et al. Downregulation by lipopolysaccharide of Notch signaling, via nitric oxide. J Cell Sci 2008;121(9):1466–1476; doi: 10.1242/jcs.019018
- 44. Bedogni B, Warneke JA, Nickoloff BJ, et al. Notch1 is an effector of Akt and hypoxia in melanoma development. J Clin Invest 2008;118(11):3660–3670; doi: 10.1172/JCI36157
- 45. Liu Z-J, Xiao M, Balint K, et al. Notch1 signaling promotes primary melanoma progression by activating mitogenactivated protein kinase/phosphatidylinositol 3-kinase-Akt pathways and up-regulating N-cadherin expression. Cancer Res 2006;66(8):4182–4190; doi: 10.1158/0008-5472.CAN-05-3589
- 46. Gurung R, Choong AM, Woo CC, et al. Genetic and epigenetic mechanisms underlying vascular smooth muscle cell phenotypic modulation in abdominal aortic aneurysm. Int J Mol Sci 2020;21(17):6334; doi: 10.3390/ijms 21176334
- Sorokin V, Vickneson K, Kofidis T, et al. Role of vascular smooth muscle cell plasticity and interactions in vessel wall inflammation. Front Immunol 2020;11:599.
- 48. Li Y, Takeshita K, Liu P-Y, et al. Smooth muscle Notch1 mediates neointimal formation after vascular injury. Circulation 2009;119(20):2686–2692; doi: 10.1161/CIRCU LATIONAHA.108.790485
- Rensen SSM, Doevendans PAFM, van Eys GJJM. Regulation and characteristics of vascular smooth muscle cell phenotypic diversity. Neth Heart J 2007;15(3):100–108.
- Zou L, Zhang J, Han J, et al. cGMP interacts with tropomyosin and downregulates actin-tropomyosin-myosin complex interaction. Respir Res 2018;19(1):201; doi: 10.1186/s12931-018-0903-z
- 51. Shvetsova AA, Borzykh AA, Selivanova EK, et al. Intrauterine nitric oxide deficiency weakens differentiation of vascular smooth muscle in newborn rats. Int J Mol Sci 2021;22(15):8003; doi: 10.3390/ijms22158003
- Dai J, Sheetz MP. Membrane tether formation from blebbing cells. Biophys J 1999;77(6):3363–3370; doi: 10.1016/S0006-3495(99)77168-7
- Hong Z, Reeves KJ, Sun Z, et al. Vascular smooth muscle cell stiffness and adhesion to collagen I modified by vasoactive agonists. PLoS One 2015;10(3):e0119533; doi: 10.1371/journal.pone.0119533
- 54. Farrell K, Simmers P, Mahajan G, et al. Alterations in phenotype and gene expression of adult human aneurysmal

- smooth muscle cells by exogenous nitric oxide. Exp Cell Res 2019;384(1):111589; doi: 10.1016/j.yexcr.2019.111589
- 55. Abdul-Hussien H, Soekhoe RGV, Weber E, et al. Collagen degradation in the abdominal aneurysm. Am J Pathol 2007;170(3):809–817; doi: 10.2353/ajpath.2007.060522
- 56. Menashi S, PoweR JT. Collagen in abdominal aortic aneurysm: Typing, content, and degradation. J Vasc Surg 1987;6(6):5.
- 57. Hinderer S, Shen N, Ringuette L-J, et al. *In vitro* elastogenesis: Instructing human vascular smooth muscle cells to generate an elastic fiber-containing extracellular matrix scaffold. Biomed Mater 2015;10(3):034102; doi: 10.1088/1748-6041/10/3/034102
- 58. Wei S, Gao L, Wu C, et al. Role of the lysyl oxidase family in organ development (Review). Exp Ther Med 2020;20(1): 163–172; doi: 10.3892/etm.2020.8731
- 59. Sun H-J, Liu T-Y, Zhang F, et al. Salusin-β contributes to vascular remodeling associated with hypertension via promoting vascular smooth muscle cell proliferation and vascular fibrosis. Biochim Biophys Acta 2015;1852(9): 1709–1718; doi: 10.1016/j.bbadis.2015.05.008
- Kolpakov V, Gordon D, Kulik TJ. Nitric oxide–generating compounds inhibit total protein and collagen synthesis in cultured vascular smooth muscle cells. Circ Res 1995; 76(2):305–309; doi: 10.1161/01.RES.76.2.305
- Mäki JM, Räsänen J, Tikkanen H, et al. Inactivation of the lysyl oxidase gene Lox leads to aortic aneurysms, cardiovascular dysfunction, and perinatal death in mice. Circulation 2002;106(19):2503–2509; doi: 10.1161/01.CIR .0000038109.84500.1E
- 62. Finney J, Moon H-J, Ronnebaum T, et al. Human copperdependent amine oxidases. Arch Biochem Biophys 2014;546:19–32; doi: 10.1016/j.abb.2013.12.022
- 63. Brophy CM, Tilson JE, Braverman IM, et al. Age of onset, pattern of distribution, and histology of aneurysm development in a genetically predisposed mouse model. J Vasc Surg 1988;8(1):45–48; doi: 10.1016/0741-5214(88) 90242-X
- 64. Umeda H, Aikawa M, Libby P. Liberation of desmosine and isodesmosine as amino acids from insoluble elastin by elastolytic proteases. Biochem Biophys Res Commun 2011;411(2):281–286; doi: 10.1016/j.bbrc.2011.06.124

- 65. Hedtke T, Schräder CU, Heinz A, et al. A comprehensive map of human elastin cross-linking during elastogenesis. FEBS J 2019;286(18):3594–3610; doi: 10.1111/febs.14929
- Horiguchi M, Inoue T, Ohbayashi T, et al. Fibulin-4 conducts proper elastogenesis via interaction with cross-linking enzyme lysyl oxidase. Proc Natl Acad Sci U S A 2009; 106(45):19029–19034; doi: 10.1073/pnas.0908268106
- 67. Robb BW, Wachi H, Schaub T, et al. Characterization of an in vitro model of elastic fiber assembly. Mol Biol Cell 1999;10(11):3595–3605; doi: 10.1091/mbc.10.11.3595
- Donato AJ, Machin DR, Lesniewski LA. Mechanisms of dysfunction in the aging vasculature and role in age-related disease. Circ Res 2018;123(7):825–848; doi: 10.1161/ CIRCRESAHA.118.312563
- 69. Fitch RM, Vergona R, Sullivan ME, et al. Nitric oxide synthase inhibition increases aortic stiffness measured by pulse wave velocity in rats. Cardiovasc Res 2001;51(2): 351–358; doi: 10.1016/S0008-6363(01)00299-1
- Nemcsik J, Kiss I, Tislér A. Arterial stiffness, vascular calcification and bone metabolism in chronic kidney disease. World J Nephrol 2012;1(1):25–34; doi: 10.5527/wjn .v1.i1.25
- 71. Blatter LA, Wier WG. Nitric oxide decreases [Ca2+]i in vascular smooth muscle by inhibition of the calcium current. Cell Calcium 1994;15(2):122–131; doi: 10.1016/0143-4160(94)90051-5

Address correspondence to: Anand Ramamurthi, PhD, FAHA Department of Bioengineering Lehigh University D325 Iacocca Hall Bethlehem, PA 18015 USA

E-mail: anr320@lehigh.edu

Received: September 19, 2022 Accepted: December 22, 2022 Online Publication Date: March 2, 2023